NTNU – Trondheim
Norwegian University of
Science and Technology

AUTONOMOUS LANDING OF UAV PATH AND NAVIGATION

Kjetil Hope Sørbø

Submission date: June 2016
Responsible professor: Thor Inge Fossen, Tor Arne Johansen

Norwegian University of Science and Technology
Department of Engineering Cybernetics

Abstract

Contents

Acronyms

ENU East North Up.

GNSS Global Navigation Satellite System.

GPS Global Positioning System.

IMC Inter-Module Communication.

MAV Miniature air vehicle.

NED North East Down.

RTK-GNSS Real Time Kinematic GNSS.

RTK-GPS Real Time Kinematic GPS.

RTKLIB Real-Time Kinematic Library.

SIL Software In the Loop.

UAS Unmanned aircraft system.

UAV Unmanned Aerial Vehicle.

Chapter 1

Introduction

1.1 Background

Recent development of flying Unmanned Aerial Vehicles (UAVs) has been recognized to provide an attractive alternative to work previously performed by manned operations. Typical work which has attracted attention includes inspection, aerial photography, environmental surveillance and search and rescue. Today UAV operation are becoming more autonomous, however in order to become fully autonomous a fixed wing UAV must be able to perform a autonomous landing.

An important premise for successful and safe UAV operation, is the provision of a robust system for safe landing of the UAV following completed operations. A autonomous landing system require a path generation system that can create a flyable landing path during flight operation from any initial position. In addition the navigation system must have centimeter level accuracy in order for the UAV to perform a autonomous landing in a net. However with a accurate navigation system the case of what to do when the positioning system degenerates must be resolved such that system failure does not occur. An other premise is that the position of the net is known, and available for the path system. With a known position of the landing net the UAV must gracefully perform a graceful decent, preferable a glide slope towards the landing net position. The length of the glide slope will be limited by the operator, which dictates that the UAV must be in the correct pose before starting the decent.

1.2 Literature review

There has been perform several studies on autonomous landing system, and there currently exist commercial available system. However these are typical expensive, and mostly focused on either military or air traffic industry. An available system for UAVs

is the SkyHook that apply INS/Global Positioning System (GPS)[Insitu], however this system require expensive equipment and is limited to a few UAV systems. The limitation on type of UAV and high cost restricts the usage of the recovery system, and motivates the research of a low cost recovery system for fixed wing UAV.

Studies that has been performed on autonomous landing has mostly focused on vision-based guidance, due to previously limited accuracy in low-cost Global Navigation Satellite System (GNSS) receiver system, which is typically single frequency receivers. In the paper [Barber et al., 2007] a landing system was proposed that compared the use of barometric pressure measurement and optic-flow measurement for estimation of height above ground. The landing path composed of a spiral path down to a given altitude where a glide slope was used to guide the MAV down to the landing area. The papers showed that optic-flow measurement reduced the average landing error with several meters, however the technique used to guided the UAV is not suitable for precision landing due to large average error from target. A low cost recovery system for fixed wing UAV is proposed in the paper [Kim et al., 2013], where computer vision is used to find and identify the recovery net. The system was successful in performing a autonomous landing, however it require that the visual image is sent from the UAV to a ground station. In addition the system require a clear image in order to calculate guidance command for the UAV, which restricts when the system can used. In the paper [Huh and Shim, 2010] a vision-based landing system is presented which was successful in performing a automatic landing. The system was aided by a standard IMU and GPS, together with a vision system relaying on color and moments based detection. The system is sensible to lighting condition, however a filtering rule was used to find the landing area. The sensibility to lighting condition is a disadvantage with vision-based guidance system, and therefore it's preferable to create a high accurate positioning system.

A net recovery system for UAV with single-frequency Real Time Kinematic GPS (RTK-GPS) was described in the paper [Skulstad et al., 2015], which was a result of the work done in the master thesis [Skulstad and Syversen, 2014]. The system presented applied RTKLIB together with low-cost single frequency GPS receivers as navigation system with a customized Ardupilot software. The complete system was able to perform a net landing, however the result showed that further work would require better controllers, and a more robust navigation system. A continuation of the work done in [Skulstad and Syversen, 2014] was done in [Frølich, 2015]. The work simulated a autonomous net landing, however no physical experiment was perform. The result in the work indicated that further work on the controllers was required, in addition to the landing path which was not suited for a Visual Line Of Sight (VLOS) UAV operation due to no spacial restrictions.

1.3 Contributions

The objective of this work is to design, implement and test a autonomous landing system for fixed wing UAV. The focus area for this work has been the design and implementation of a landing plan, and a high accurate navigation system. The landing path generator is a improved version of the landing path used in [Skulstad and Syversen, 2014] moved into the DUNE environment, and combined with the landing path generator interface created in the master thesis [Frølich, 2015]. The navigation system continues the work started in the master thesis [Spockeli, 2015], where Real Time Kinematic GNSS (RTK-GNSS) was made available to the DUNE environment. The guidance and control system used during the testing of the system was developed at the UAVLab by a fellow master student. The contributions of this thesis are a landing plan generator, a navigation system able to provide high accurate position and velocity information, a redundancy strategy for short loss of RTK-GNSS, a mobile sensor unit used as a GPS reference location for net placement and a experimental testing and operational study of the autonomous landing system, summarised as follows:

1. **A landing plan generator** has been created, which guaranty a flyable path from any initial position to a landing zone, with a specified decent angle. The landing plan generator has been implemented in the DUNE runtime environment, which is capable to be used in both a stationary and moving net landing. In addition to the implementation of the landing plan a **Application Programming Interface (API)** has been created to generate a landing plan.
2. **A navigation state control system** has been created to manage which positioning system should be used in the DUNE environment. The state machine is designed to switch between the position and velocity information provided by the external navigation system and the RTK-GNSS position and velocity solution.
3. **Increased the robustness of the RTK-GPS** by creating a bias estimator, which estimate the bias between RTK-GPS and a standalone GPS. The bias is used to compensate the external navigation position solution such that the external navigation position solution equals a FIX RTK-GNSS position solution.
4. **A navigation state monitor interface** has been created to provide a visual indicator of which navigation system that is used in the DUNE environment. The monitor is color coded such that changes in the state of the navigation system detected with more ease.
5. **A mobile sensor with RTK-GPS** has been created to be a reference position for a stationary net. The mobile sensor unit can be place on a runway, and used

as a reference point for net placement in the command and control monitor, and provide accurate position solution for placement of net through the use of RTK-GNSS.

6. **Experimental testing** of the navigation system and landing path generator in the field. The autonomous landing system was tested on the Agdenes airfield with a virtual net placed $25m$ above the runway. Test result gathered from the field test has been used in a **operational study** on performance and feasibility of a autonomous landing at Agdenes airfield.

1.4 Outline

Chapter 2 outlines two path planing strategies which is used in the development of the landing path system. The chapter also contains a model of a Miniature air vehicle (MAV).

Chapter 3 proposes a path and navigation system for a autonomous landing system. The landing path system is separated into two planes, which is the lateral and longitudinal plane. The lateral path is created as a Dubins path, and the longitudinal path is created as a straight line path. The navigation system is controlled by a state machine which controls the source of the positioning and velocity solution, in addition to increasing the robustness of the RTK-GNSS.

Chapter 4 outlines the software used to create and test the autonomous landing system as well as the hardware configuration used as a basis for the X8 fixed wing UAV.

Chapter 5 outlines the implementation details of the path and navigation system, including simulation verification of the system.

Chapter 6 present experimental testing of the path and navigation system in the field

Chapter 7 present the closing discussion with conclusion and recommendation for further work.

Chapter 2

Basis and modelling

2.1 UAV model

A UAV model is presented in [Beard and McLain, 2012], which present the kinetic equations of a general MAV in the. The kinetic equations is given in the body frame, which is fixed to the frame of the UAV. The kinematics equations is given as:

$$\begin{bmatrix} \dot{x} \\ \dot{y} \\ \dot{z} \end{bmatrix} = \mathbf{R}(\mathbf{\Theta})_{Body}^{NED} \begin{bmatrix} u \\ v \\ w \end{bmatrix} \tag{2.1a}$$

$$\begin{bmatrix} \dot{\phi} \\ \dot{\theta} \\ \dot{\psi} \end{bmatrix} = \mathbf{T}(\mathbf{\Theta}_{nb}) \begin{bmatrix} p \\ q \\ r \end{bmatrix} \tag{2.1b}$$

where $\mathbf{R}(\mathbf{\Theta})_{Body}^{NED}$ is the rotation matrix from the body frame to the NED frame, with $\mathbf{\Theta} = \begin{bmatrix} \phi & \theta & \psi \end{bmatrix}^T$. The transformation matrix $\mathbf{T}(\mathbf{\Theta}_{nb})$ is given in [Fossen, 2011] as:

$$\mathbf{T}(\mathbf{\Theta}_{nb}) = \begin{bmatrix} 1 & \sin(\phi)\tan(\theta) & \cos(\phi)\tan(\theta) \\ 0 & \cos(\phi) & -\sin(\phi) \\ 0 & \frac{\sin(\phi)}{\cos(\theta)} & \frac{\cos(\phi)}{\cos(\theta)} \end{bmatrix} \tag{2.2}$$

The kinetic equations is given as:

$$\begin{bmatrix} F_x \\ F_y \\ F_z \end{bmatrix} = \mathbf{R}(\mathbf{\Theta})_{NED}^{Body} \begin{bmatrix} 0 \\ 0 \\ mg \end{bmatrix} - \frac{1}{2}\rho V_a^2 S \mathbf{R}(\alpha)_{Stability}^{Body} \begin{bmatrix} F_{Drag} \\ 0 \\ F_{Lift} \end{bmatrix} \tag{2.3a}$$
$$+ \frac{1}{2}\rho V_a^2 S \begin{bmatrix} 0 \\ C_y(\beta, p, r, \delta_a, \delta_r) \\ 0 \end{bmatrix} + \frac{1}{2}\rho S_{Prop} C_{Prop} \begin{bmatrix} (K_{Motor}\delta_t)^2 - V_a^2 \\ 0 \\ 0 \end{bmatrix}$$
$$\begin{bmatrix} L \\ M \\ N \end{bmatrix} = \frac{1}{2}\rho V_a^2 S \begin{bmatrix} C_L(\beta, p, r, \delta_a, \delta_r) \\ C_M(\alpha, q, \delta_e) \\ C_N(\beta, p, r, \delta_a, \delta_r) \end{bmatrix} + \begin{bmatrix} -k_{T_p}(K_\Omega \delta_t)^2 \\ 0 \\ 0 \end{bmatrix} \tag{2.3b}$$

where ρ is the air density in kg/m^3,mg is the weight of the UAV, S is the platform area of the MAV wing, C_i is nondimensional aerodynamic coefficients and V_a is the speed of the MAV through the surrounding air. α and β is the attack and side slip angle respectfully. F_{Drag} is the drag force acting on the fuselage, and F_{Lift} is the lift force. $\mathbf{R}(\alpha)_{Stability}^{Body}$ is the rotation matrix from the stability frame to the body frame. The stability frame is orientated with respect to the MAV movement through the surrounding air, which is defined as a standard rotation around the y-axis of the body frame. S_{Prop} is the area swept out by the propeller, and K_{Motor},K_{T_p} and K_Ω is propeller specific constants. The control surface on the MAV is defined into two groups; the wings and the rudder. On the rudder δ_e controls the elevator deflection and δ_r the rudder deflection. For the wings δ_a is the control input from the aileron deflection. The control input for the control input is δ_t.

2.2 Landing path modelling

A landing path is a path following problem where the minimum requirement is that the path is connected, and is flyable. The connection level can be described by the paths smoothness. Smoothness can be described with parametric continuity, which is denoted C^n were n is the degree of smoothness. The order of n implies that the n first parametric derivatives match at a common point for two subsequent paths [Barsky and DeRose, 1989]. Geometric continuity is a relaxed from of parametric continuity in which discontinuousness in speed is allowed. A table 2.1 of geometric and parametric continuity lists the requirement for each smoothness level, which is based definitions presented in [Barsky and DeRose, 1989]. Geometric continuity is sufficient for a path following system, which is the main focus of this thesis. Geometric continuity is denoted as G^n were n is the order of continuity.

Geometrical smoothness level	**Description**
G^0	All subpaths are connected
G^1	The path-tangential angle is continuous
G^2	The center of curvature is continuous
Parametric smoothness level	**Description**
C^0	All subpaths are connected
C^1	The velocity is continuous
C^2	The acceleration is continuous

Table 2.1: Smoothness definitions

The definition used for path in this thesis is equation 1.2 in [Tsourdos et al., 2010] which state:

$$P_s(x_s, y_s, z_s, \theta_s, \psi_s) \xrightarrow{r(\varpi)} P_f(x_f, y_f, z_f, \theta_f, \psi_f) \tag{2.4}$$

where the subscripts s and f denotes the start pose and finish pose respectfully with $r(\varpi)$ as the path and ϖ the path variable.

2.2.1 Straight lines

The simplest form on path is a straight line between P_s and P_f. For simplicity the path is reduced to a 2 dimensional case, where the straight line is given as

$$x(\varpi) = a_x\varpi + b_x \tag{2.5a}$$
$$y(\varpi) = a_y\varpi + b_y \tag{2.5b}$$

with $\varpi \in [0, 1]$, where ϖ has not necessary a physical meaning. Then the parametrisation of the straight line is:

$$P(0) = \begin{bmatrix} x(0) \\ y(0) \end{bmatrix} = \begin{bmatrix} b_x \\ b_y \end{bmatrix} = \begin{bmatrix} x_s \\ y_s \end{bmatrix} \tag{2.6a}$$
$$P(1) = \begin{bmatrix} x(1) \\ y(1) \end{bmatrix} = \begin{bmatrix} a_x + b_x \\ a_y + b_y \end{bmatrix} = \begin{bmatrix} x_f \\ y_f \end{bmatrix} \rightarrow \begin{bmatrix} a_x \\ a_y \end{bmatrix} = \begin{bmatrix} x_f - b_x \\ y_f - b_y \end{bmatrix} \tag{2.6b}$$

The tangential vector for a straight line is given as:

$$\psi(\varpi) = \text{atan2}(a_y, a_x) \tag{2.7}$$

with it's derivative:

$$\dot{\psi}(\varpi) = 0 \tag{2.8}$$

A path constructed by straight lines is G^0, however since the tangential vectors derivative is zeros, it is discontinuous between two line segments with different heading and therefore not G^1[TODO: LEGG INN FIGUR SOM VISER DISKONINUITETEN]. The disadvantage with a path which is G^0 is that large discontinuity between two tangential vectors will cause problem for a control system.

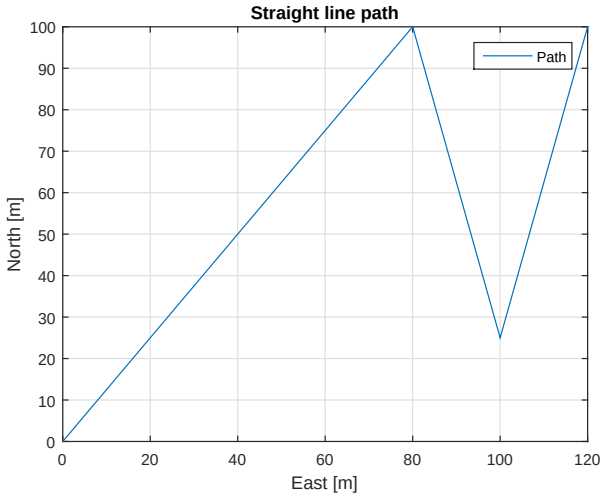

Figure 2.1: Straight line path

2.2.2 Dubins path

An alternative to a straight line path is a path constructed by straight lines and circle. Such a path is Dubins path[Dubins, 1957], which showed that the shortest possible path for a particle that moved with unit speed with maximum curvature would consist of two circles and a straight line which is tangential to both circles. A disadvantage with Dubins path is that the curvature is discontinues, which gives a path from P_s to P_f with smoothness level of G^1.

A Dubins path that is constructed where the final orientation is fixed has four different ways to be constructed, which is determined by the rotation directions. The four types of Dubins path that is used in this thesis is given in table 2.2.

Right to Right
Right to left
Left to Right
Left to left

Table 2.2: Turning direction for Dubins path with fixed final orientation

The equations that is used to construct the path is found in [Tsourdos et al., 2010] section 2.2.1, with a constructed path shown in figure 2.2. In figure 2.2 the whole line is the path, with the doted lines used to constructed the path.

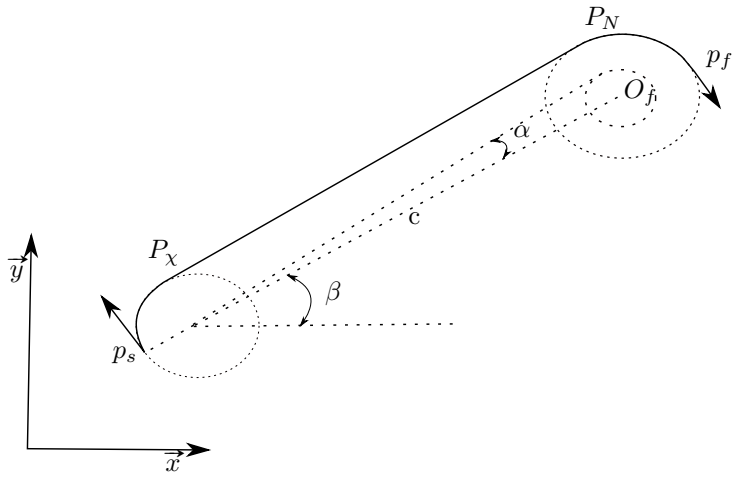

Figure 2.2: Dubins path

The first step if to determine the start and final turning circle center. The center is found with the equations:

$$X_{cs} = X_s - R_s \cos(\psi_s \pm \frac{\pi}{2}) \tag{2.9a}$$

$$Y_{cs} = Y_s - R_s \sin(\psi_s \pm \frac{\pi}{2}) \tag{2.9b}$$

$$X_{cf} = X_f - R_f \cos(\psi_f \pm \frac{\pi}{2}) \tag{2.9c}$$

$$Y_{cf} = Y_f - R_f \sin(\psi_f \pm \frac{\pi}{2}) \tag{2.9d}$$

where R_s and R_f is the radius of the start and final turning circle respectfully, with ψ_s and ψ_f the start and final heading. The centres for the start and final turning circle is defined as:

$$\mathbf{O}_{cs} = \begin{bmatrix} X_{cs} \\ Y_{cs} \end{bmatrix} \tag{2.10}$$

$$\mathbf{O}_{cf} = \begin{bmatrix} X_{cf} \\ Y_{cf} \end{bmatrix} \tag{2.11}$$

Continuing the centres O_{cs} and O_{cf} is connected with a centreline c, where the length is given as:

$$|c| = ||\mathbf{O}_{cs} - \mathbf{O}_{cf}||_2 \tag{2.12}$$

where $||\cdot||_2$ is the second norm. Continuing the arc exit and entry point for the start and final circle is calculated by first applying the equations:

$$\alpha = \arcsin\left(\frac{R_f - R_s}{|c|}\right) \tag{2.13a}$$

$$\beta = \arctan\left(\frac{Y_{cf} - Y_{cs}}{X_{cf} - X_{cs}}\right) \tag{2.13b}$$

where α is the angle between the length of the center line between the two circles, and the length of the line from the start circle to the exit tangent point. β is the angle of the center line with respect to the inertial frame. The exit and entry tangent point is found with the use of table 2.3.

	Turn angle
ϕ_{right}	$\alpha + \beta + \frac{\pi}{2}$
ϕ_{left}	$\beta - \alpha + \frac{3\pi}{2}$

Table 2.3: Turn angle

With the angle of the exit and entry tangent point the point is given as:

$$x_{P_\chi} = x_{cs} + R_s\cos(\phi) \tag{2.14a}$$

$$y_{P_\chi} = x_{cs} + R_s\sin(\phi) \tag{2.14b}$$

$$x_{P_N} = x_{cf} + R_f\cos(\phi) \tag{2.14c}$$

$$y_{P_N} = x_{cf} + R_f\sin(\phi) \tag{2.14d}$$

which is used to define the exit and entry points as:

$$\mathbf{P}_\chi = \begin{bmatrix} x_{P_\chi} \\ y_{P_\chi} \end{bmatrix} \tag{2.15a}$$

$$\mathbf{P}_N = \begin{bmatrix} x_{P_N} \\ y_{P_N} \end{bmatrix} \tag{2.15b}$$

The length of the path is calculated in three parts. The first the is the arc length from the start pose to the exit tangent point, then the length of the straight line before the arc length from the entry point to the final pose. The length of the path is given as:

$$d = R_s\phi_s + d_t + R_f\phi_f \tag{2.16}$$

where $d_t = ||\mathbf{P}_N - \mathbf{P}_\chi||_2$, ϕ_s and ϕ_f is the arc angle for the start and final circle respectfully.

Chapter 3

Path and Navigation

3.1 Path system

The path system consist of two main parts, which the landing path and the approach path. The landing path is a straight line path orientated with respect to a reference net position. The approach path is design separately as a lateral Dubins path and a longitudinal straight line path. The approach path is designed to ensure that the UAV is able to enter the landing path at the correct height with the correct attitude.

3.1.1 Landing Path

The landing path is inspired by the work done in [Skulstad and Syversen, 2014] where waypoint was used to create a straight line path towards the net. This method proved successful, and thus this landing system continues on the work. The angles in the straight line path must be kept small to avoid large transition behaviour from switching way-point, however the trade off is that the start high in of the landing path must be above any obstacles that is around the landing area. At sea this could be other ships or platforms, and on land it could be threes or hills. The straight line path is constructed relative to the net as shown in figure 3.1, with way-points given

as:

$$\mathbf{WP4} = \begin{bmatrix} -a0 \\ 0 \\ h_{nc} + a1\tan(\gamma_n) \end{bmatrix} \tag{3.1a}$$

$$\mathbf{WP3} = \begin{bmatrix} a1 \\ 0 \\ h_{nc} - a1\tan(\gamma_n) \end{bmatrix} \tag{3.1b}$$

$$\mathbf{WP2} = \mathbf{WP3} + \begin{bmatrix} a2 \\ 0 \\ -a2\tan(\gamma_l) \end{bmatrix} \tag{3.1c}$$

$$\mathbf{WP1} = \mathbf{WP2} + \begin{bmatrix} a3 \\ 0 \\ 0 \end{bmatrix} \tag{3.1d}$$

where the description of the parameters used is given in table 3.1. The net is placed between the fourth and third way points such that transitional behaviour do not occur during the finale stage of the net landing.

Parameter	**Description**
h_{nc}	The height from ground to the net center
$a0$	The distance behind the net
$a1$	The distance in front of the net
$a2$	The length of the glide slope
$a3$	The length of the approach towards the glide slope
γ_n	The net attack angle
γ_l	The landing glide slope angle

Table 3.1: Net approach parameters

The way point vectors are rotated into the NED frame by a rotation around the z-axes.

$$\mathbf{WP}^n = \mathbf{R}(\psi_{net})\mathbf{WP}^b \tag{3.2}$$

were ψ_{net} is the heading of the net, and $\mathbf{R}(\psi_{net})$ is the standard rotation matrix around the z-axis.

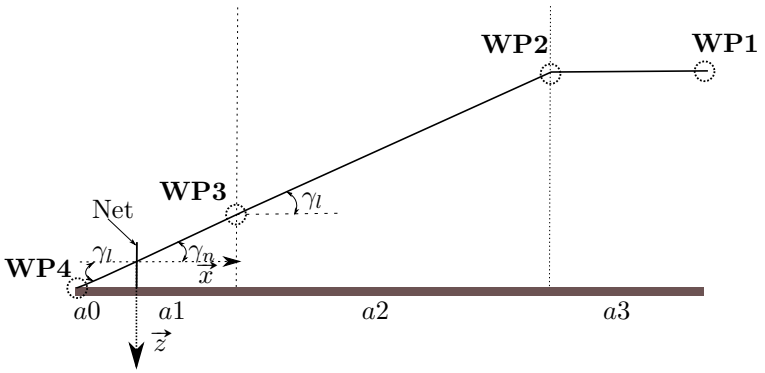

Figure 3.1: The landing path

3.1.2 Approach path

The landing path is separated into two parts, which is a lateral and longitudinal path. The purpose of the path is to ensure that the UAV can enter the landing path at the correct height with the correct attitude from any initial position. The lateral and longitudinal path are created separately

Lateral path

The lateral path is designed as a Dubins path, with start pose, P_s, at the point where the landing plan generation request was made, and final pose, P_f, at the start of the landing path. Dubins path was chosen since it can be followed by a UAV, and meet the requirement that the UAV enters the landing path with the correct heading.

The lateral path is constructed following the equations in section 2.2.2, however the rotation direction in each circle must first be determined. The desired behaviour is to find the shortest path of the four different rotation pairs given in table 2.2. The shortest path is determined by calculating the length of each variants, where the shortest is chosen. The resulting the path is shown in figure 3.2.

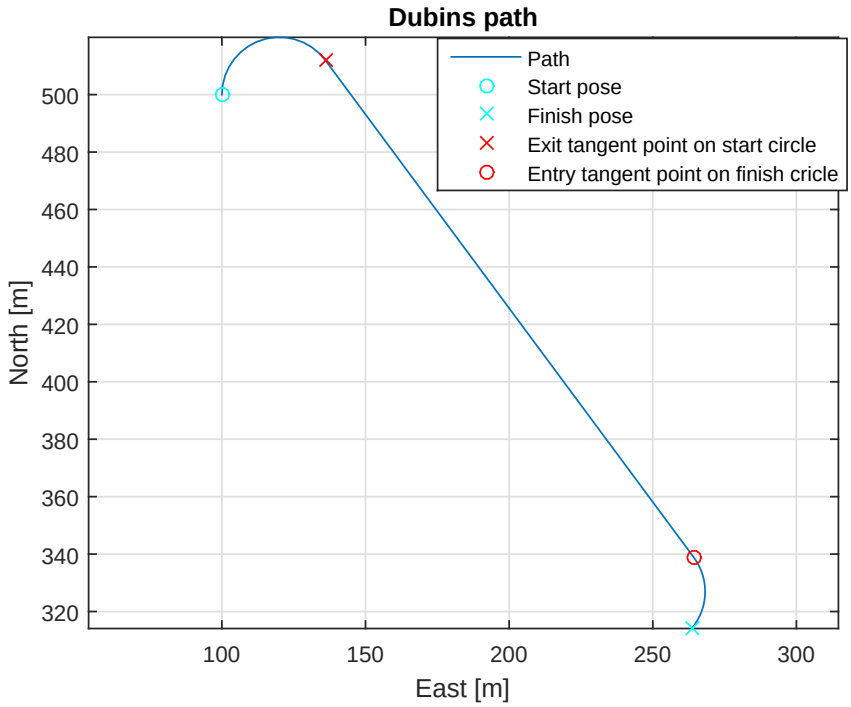

Figure 3.2: Lateral Dubins path

The construction of the lateral path consists of two arc with a straight line between the arcs. The arcs are constructed by first finding the start and finish heading defined as ψ_0 and ψ_1 respectfully:

$$\psi_0 = \begin{cases} \text{atan2}(Y_s - Y_{cs}, X_s - X_{cs}) & \text{if start circle} \\ \text{atan2}(Y_{P_N} - Y_{cf}, X_{P_N} - X_{cf}) & \text{otherwise} \end{cases} \tag{3.3a}$$

$$\psi_1 = \begin{cases} \text{atan2}(Y_{P_\chi} - Y_{cs}, X_{P_\chi} - X_{cs}) & \text{if start circle} \\ \text{atan2}(Y_f - Y_{cf}, X_f - X_{cf}) & \text{otherwise} \end{cases} \tag{3.3b}$$

Continuing the turn angle must be defined, which is the difference between ψ_1 and ψ_0. However the periodic behaviour of the unit circle must respected, including the rotation direction. The maximum turning angle becomes:

$$\psi_{max} = \begin{cases} -|\psi_1 - \psi_0| & \text{if counter clockwise rotation and } \psi_1 - \psi_0 \leq 0 \\ -(2\pi - |\psi_1 - \psi_0|) & \text{if counter clockwise rotation and } \psi_1 - \psi_0 > 0 \\ |\psi_1 - \psi_0| & \text{if clockwise rotation and } \psi_1 - \psi_0 \geq 0 \\ (2\pi - |\psi_1 - \psi_0|) & \text{if clockwise rotation and } \psi_1 - \psi_0 < 0 \end{cases} \tag{3.4}$$

where $\psi_1 - \psi_0 \in (-\pi, \pi]$. From the maximum turning angle the angle step and number of angle segments in the arc can be determined:

$$h = \frac{d_{arc}}{R} \tag{3.5a}$$

$$N = \left\lceil \frac{\text{sign}(\psi_{max})\psi_{max}}{h} \right\rceil + 1 \tag{3.5b}$$

$$h = \text{sign}(\psi_{max})h \tag{3.5c}$$

where h is arc angle step and N the total number of steps in the arc. The step angle must have the same sign as ψ_{max} to ensure the correct rotation direction. Continuing the heading function $\psi(\varpi)$ can be defined as:

$$\psi(\varpi) = \begin{cases} \psi_{max} & \varpi = N - 1 \\ \varpi h & \text{otherwise} \end{cases} \tag{3.6}$$

where $\varpi = 1, ..., N - 1$. Finally the arc path can be defined as:

$$\mathbf{p}(\varpi) = \begin{bmatrix} \mathbf{O}_c \end{bmatrix} + R \begin{bmatrix} \cos(\psi_0 + \psi(\varpi)) \\ \sin(\psi_0 + \psi(\varpi)) \end{bmatrix} \tag{3.7}$$

A summary of the lateral path is:

$$\mathbf{p}(i) = \begin{cases} \begin{bmatrix} \mathbf{O}_{cs} \end{bmatrix} + R_s \begin{bmatrix} \cos(\psi_0 + \psi(\varpi)) \\ \sin(\psi_0 + \psi(\varpi)) \end{bmatrix} & \text{Start circle} \\ \begin{bmatrix} \mathbf{O}_{cf} \end{bmatrix} + R_f \begin{bmatrix} \cos(\psi_0 + \psi(\varpi)) \\ \sin(\psi_0 + \psi(\varpi)) \end{bmatrix} & \text{Finish circle} \end{cases} \tag{3.8}$$

where $i = \varpi_s + \varpi_f$ with ϖ_s and ϖ_f as the number of segments in the start and finish circle respectfully.

Longitudinal path

The longitudinal path is designed as a straight line along the lateral path, which results in a spiral path in the arcs created by the lateral path. The approach path hold a constant decent angle until the correct height is reached, which is defined as the start height for the landing path. The approach decent angle is then accused such that the correct height is reach. The approach decent angle is defined as:

$$\gamma_d = \begin{cases} \text{atan2}(\Delta z, ||\mathbf{p}(i+1) - \mathbf{p}(i)||_2) & \text{if } \text{atan2}(\Delta z, ||\mathbf{p}(i+1) - \mathbf{p}(i)||_2) \leq \gamma_{d_{Max}} \\ \gamma_{d_{Max}} & \text{otherwise} \end{cases} \tag{3.9}$$

where $\gamma_{d_{Max}}$ is the maximum decent angle for the approach path, and Δz is defined as:

$$\Delta z = z_d - z(i) \tag{3.10}$$

where z_d is the z component in $WP1$. Continuing the longitudinal path is given as:

$$\mathbf{r}(i+1) = \begin{bmatrix} \mathbf{p}(i) \\ ||\mathbf{p}(i+1) - \mathbf{p}(i)||_2 \tan(\gamma_d) \end{bmatrix} \tag{3.11}$$

where $\mathbf{r}(i)$ is the landing path and $p = \begin{bmatrix} x(i) & y(i) \end{bmatrix}^T$ is the lateral path. The resulting height profile of the approach path is shown in figure 3.3.

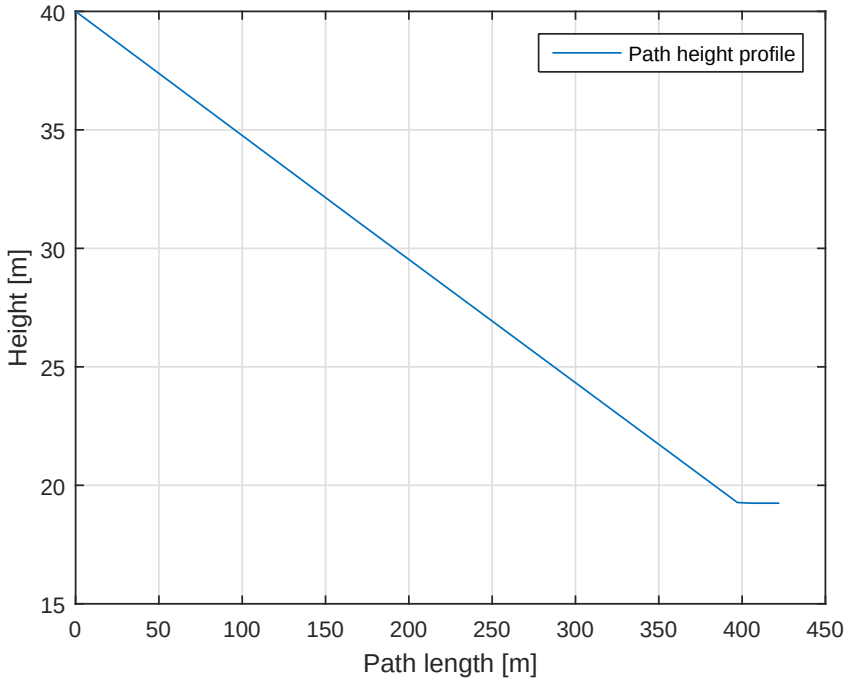

Figure 3.3: Height profile of the landing path

Spiral path The longitudinal path will in the case where the correct height is not reach enter a spiral such that the correct height is reached. The spiral keeps the same turn radius as the finish circle in the lateral path. The longitudinal path continues along the spiral until the correct height can be reached with and decent angle equal or less then $\gamma_{d_{Max}}$. Continuing an arc is created such that the path ends with the correct heading. The arc has the same rotation direction as the lateral path, with start point where the correct height was reached and end point of the start of the

landing path. The complete approach path combined with the landing path is shown in figure 3.2.

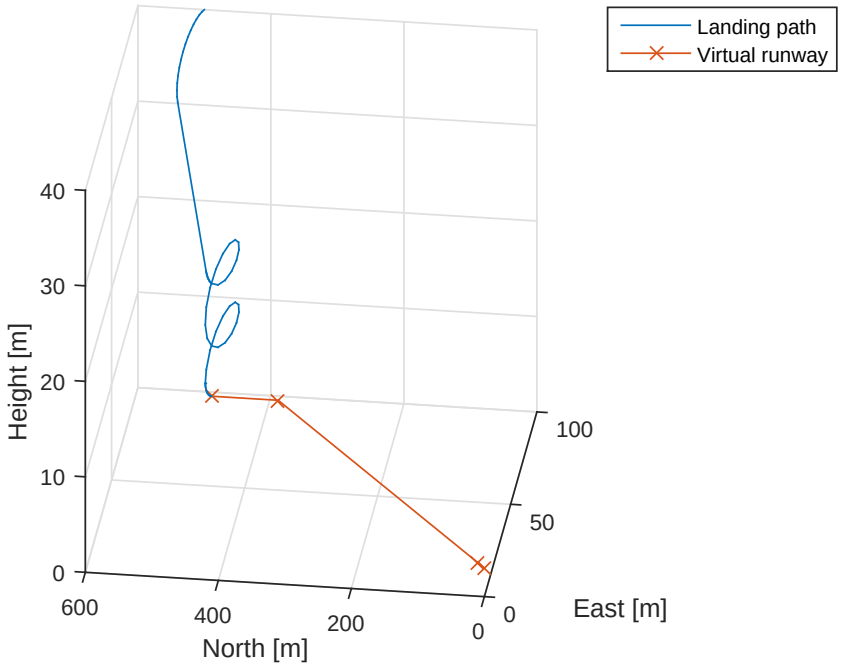

Figure 3.4: Approach path connected to the landing path

3.2 Navigation system

The navigation system consist of two position and velocity measurement system, where one is a high accurate positioning system and the other a reliable backup system. The high accurate positioning system apply RTK-GPS, which is able to provide high accurate position solution. The backup positioning system consist of a standard package of standalone GPS and Inertial Measurement Unit (IMU) together with a Kalman filter, which is a proven reliable system in Ardupilot together with a Pixhawk. Ardupilot and Pixhawk are explained further in section 4.4 and section 4.3. However the RTK-GPS is subject to drop out, which create a situation where the navigation system should switch to standalone GPS or wait for the RTK-GPS to return. A state machine has been created to handle the state switching between RTK-GPS and the external navigation data, which is navigation data from the Pixhawk. This is handled in two steps. The first is a short loss compensator stage, where the backup standalone GPS is compensated to get a position solution closer to

the RTK-GPS solution. The second stage fully disconnect the RTK-GPS. First the term RTK-GPS will be further explained, together with typical error sources that affect a GNSS positioning system.

3.2.1 Position estimation RTK-GPS

Real Time Kinematic GPS (RTK-GPS) is in [Misra and Enge, 2011] section 7.2.2 defined as a rover that receive raw GNSS measurements from a reference receiver which is transmitted over a radio link. A key feature with RTK-GPS is that the rover is able to estimate the integer ambiguities while moving. The reference receiver is usually defined as a base station, and the integer ambiguity is the uncertainty of the number of whole phase cycles between the receiver and a satellite. With the measurements from the base station the rover is able to calculated the distance between itself and the base station, where the distance is referred to as a baseline. The length of the baseline affect the accuracy of the RTK-GPS solution, due to increased effect of atmospheric disturbance, which is further explain in 3.2.1. However with a short baseline, e.g. $1 - 2km$, the atmospheric condition can be considered equal for the base station and the rover, which keeps the solution at centimetre level accuracy. The concept of RTK-GPS is depicted in figure 3.5.

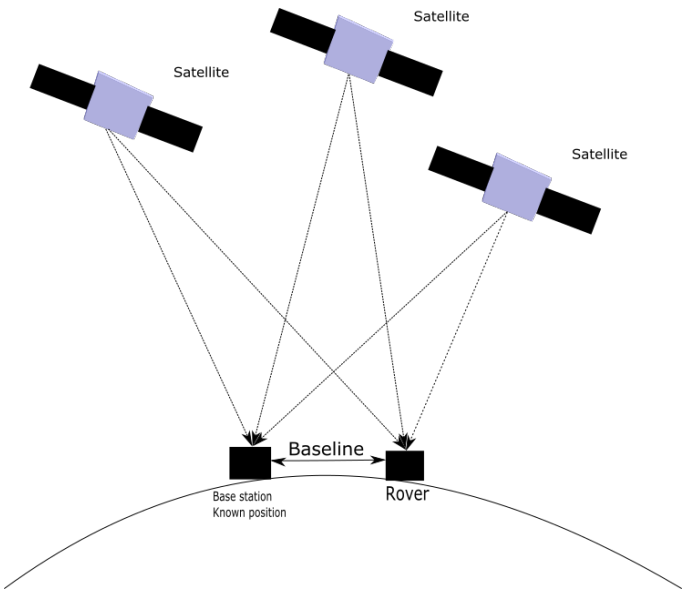

Figure 3.5: Concept figure of Real Time Kinematic GPS (RTK-GPS)

The ability for the rover to resolve the integer ambiguity is a key feature in RTK-GPS. A well used method was purposed in the article [Teunissen, 1994] which

decorrelate the integer ambiguities such that a efficient computation of the least square estimate can be performed. The search method is further explained in [Teunissen, 1995]. A estimate of the integer ambiguity with sufficient high degree of certainty is referred to as a FIX solution, otherwise the solution is degraded to FLOAT where the integer ambiguity is allowed to be a decimal or a floating point number. When the solution is categorised as FIX the accuracy of the solution is considered on centimetre level, while with a FLOAT solution the accuracy is at a decimetre level. However when a FIX solution is lost, the solution accuracy will not imminently degrade to decimetre level.

In RTK-GPS the position of the base station must be resolved. This can be achieved by either knowing the position beforehand, which is defined as a kinematic configuration. If the base station position is unknown the RTK-GPS solver calculates the position on the fly, which is defined as a moving baseline configuration. The unknown position is then calculated as a standalone GNSS receiver, with the accuracy that entails. Therefore the RTK-GPS system with a moving baseline configuration can never have better global accuracy then what it will get with a single receiver. The advantage with the moving baseline configuration is that the base station is allowed to moved, and with RTK-GPS the relative position between the rover and base station can be determined in real time. This will be the case in automatic ship landing system, where the base station is on a ship, thus must be allowed to move. The advantage with kinematic mode is that it can give a more accurate position estimate, however this require that the base station is known and stationary.

Error sources

In order to get high accuracy in the position estimation the different error sources must be identified and removed if possible. This section will identify some of the most significant error sources that can affect the GNSS signal, and how to remove or mitigate them in the estimation.

Clock error There is drift in both the satellite clock and the receiver clock. The atomic clock in the satellites makes the clock drift negligible from the user perspective. The receiver clock tend to drift, and if not taken into account will cause large deviations in the position estimate from the true position. This error is remove by including a fourth satellite in the position computation. The satellite clock error is given in the satellite message.

Ionospheric and tropospheric delays When the GPS signals travel though the atmosphere there will be a delay caused by the different atmospheric layers. The atmosphere change the velocity of wave propagation for the radio signal, which results in altered transit time of the signal.

Ionospheric delay Gas molecules in the ionosphere becomes ionized by the ultraviolet rays that is emitted by the sun, which release free electrons. These electron can influence electromagnetic wave propagation, such as GNSS signals. In [Vik, 2014] section 3.5.1 it's stated that the delay caused by the ionosphere usually is in the order of $1 - 10$meters. The error can be mitigated by using a double frequency receiver, or by applying a mathematical model to estimate the delay. Both those methods are with a single receiver, however by including a second receiver in a network, e.g. RTK-GPS, the GNSS solution system can assume that both receiver receive signal in the same epoch, which means that the signals have experienced the same delay. The rover is then able to remove the error induced from ionospheric disturbance.

Tropospheric delay The tropospheric delay is a function of the local temperature, pressure and relative humidity. The effect of tropospheric delay can vary from 2.4 meters to 25 meters depending on the elevation angle of the satellites,[Vik, 2014] section 3.5.1. The error can be mitigated by applying a mathematical model to estimate the tropospheric delay, or by using a elevation mask can remove all satellites with a elevation angle bellow a certain threshold. Similar to ionospheric delay, tropospheric delay can be removed when using two receivers in a network by assuming that the single received by both receivers has experienced the same delay. The tropospheric delay is a function of the local temperature, pressure and relative humidity. The effect of tropospheric delay can vary from 2.4 meters to 25 meters depending on the elevation angle of the satellites,[Vik, 2014] section 3.5.1. The error can be mitigated by applying a mathematical model to estimate the tropospheric delay, or by using a elevation mask can remove all satellites with a elevation angle bellow a certain threshold. Similar to ionospheric delay, tropospheric delay can be removed when using two receivers in a network by assuming that the single received by both receivers has experienced the same delay.

Multipath One of the primary source of error in in a GNSS receiver is multipath. Multipath happens when the satellite signal is reflected by a nearby surface before if reach the GNSS antenna. The delay introduced in the signal can make the receiver believe that its position is several meters away form its true position. The easiest way to mitigated multipath is to place the antenna at a location with open skies, with no tall structures nearby. The effect can also be mitigated by choosing a antenna with good multipath rejection capability.

Multipath error uncorrelated between receivers, thus the local receiver must be able to correct for multipath error locally.

3.2.2 Navigation state control system

The navigation state control system manage the current state of the navigation system, which controls if the RTK-GPS usage and responsible of dispatching the current state of the UAV to the rest of the DUNE system. The structure of the navigation state control system is shown in figure 3.6, with edge description given in table 3.2. The basic state of the navigation system function as if the RTK-GPS system is not available, which makes the navigation system independent from the RTK-GPS system. This is a requirement for the navigation system since it should function in a UAV where RTK-GPS is not present.

In order for the navigation system to switch state into "Rtk ready" the RTK-GPS message must contain a valid base position, which must be set by the user. The setting of the base station is specified further in section 5.2.1. In addition the RTK-GPS solution type must be valid for x seconds such that a stable desired solution type is available.

The navigation state control system will only use the RTK-GPS system if the user has configured the navigation system to apply RTK-GPS and if it's available.

The state machine can enter a state during loss of RTK-GPS, where the position solution from the Pixhawk is compensated with the average difference between the RTK-GPS position solution and the Pixhawk solution. This state will be further explained in section 3.2.2.

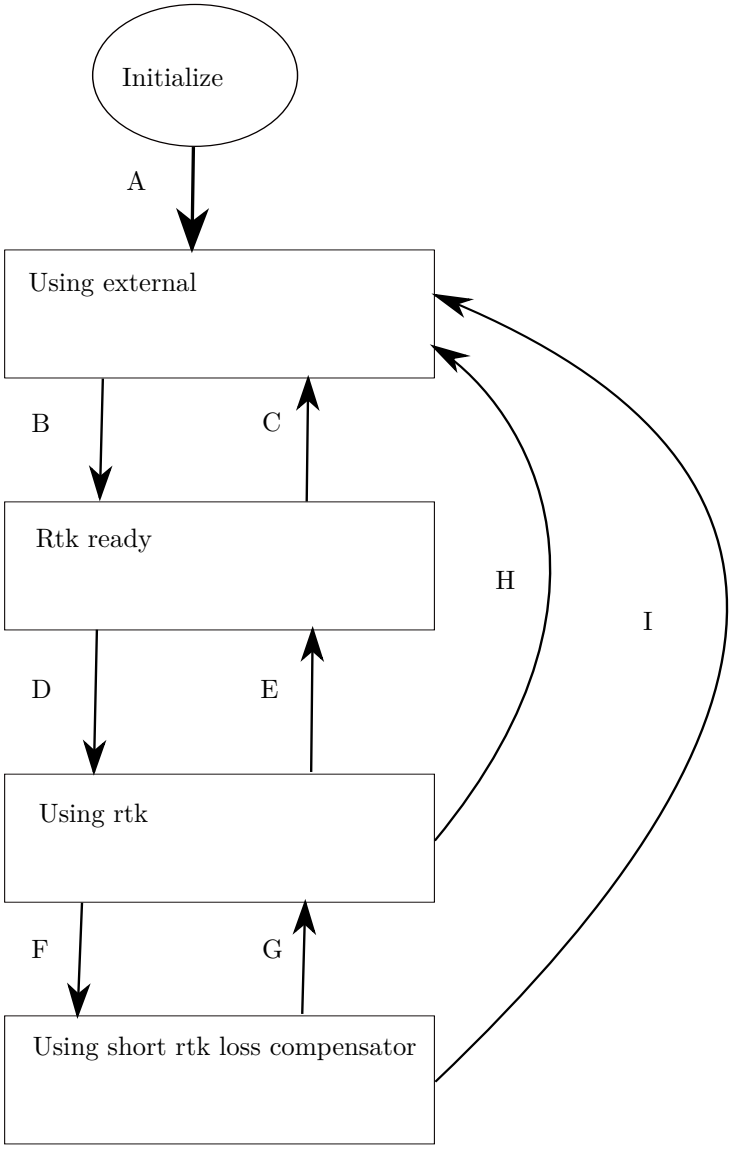
Initialize
A
Using external
B
C
Rtk ready
H
I
D
E
Using rtk
F
G
Using short rtk loss compensator

Edge	Event	Guard
A	Event: Received External Nav message	None
B	Time out: Fix RTK-GPS solution for x seconds with valid base position	None
C	Time out: x seconds since last valid GpsFixRtk	None
D	Flag: Using Rtk is set true	None
E	Flag: Using Rtk is set false	None
F	Time out: x seconds since last valid GpsFixRtk Event: Received GpsRtkFix with type == None	Short loss compensator: Enabled
G	Event: Received valid GpsFixRtk message	None
H	Time out: x seconds since last valid GpsFixRtk Event: Received GpsRtkFix with type == None	Short loss compensator: Disabled
I	Time out: x seconds since last valid GpsFixRtk	None

Table 3.2: Description of the edges used in the state machine

The state machine is designed to alter behaviour when the state machine enters a new state, with the entries action listed in table 3.4. A summary of the states in the navigation state control system is given in table 3.3.

State	Description
Initialize	The task starting up
Using external	The navigation task apply the external navigation source in the state message
RTK ready	The RTK-GPS is ready for use, however the external navigation source is still used
Using RTK	The navigation task apply the RTK-GPS in the state message
Using short RTK loss compensator	The navigation task apply the external navigation source with a compensation term to reduce the effect of RTK-GPS loss.

Table 3.3: States in the navigation system with description

State	**Entry action**
Initialize	Start up for the navigation state control system
Using external	RTK-GPS is disabled Availability activation timer for RTK-GPS is started State of navigation system is updated
RTK ready	RTK-GPS is disabled Availability deactivation timer for RTK-GPS is started State of navigation system is updated
Using RTK	RTK-GPS is enabled State of navigation system is updated If short RTK loss compensator is activated: - Short RTK loss compensator activation timer is started If short RTK loss compensator is deactivated: - RTK-GPS time out timer is started
Using short RTK loss compensator	Short RTK loss compensator deactivation timer is started

Table 3.4: Entry action for each state

Short loss of RTKGPS

In order for the navigation system to handle short loss of RTK-GPS a short loss RTK-GPS system is presented. The compensator is based on that the position solution from the external navigation system is almost constant with respect to the RTK-GPS solution. Therefore the average difference between the RTK-GPS position solution and the external navigation system should be able to move the external navigation position solution closer to the RTK-GPS position solution. The short loss compensator is given as:

$$\mathbf{e}(n) = \mathbf{p}_1(n) - \mathbf{p}_2(n) \tag{3.12}$$

$$\delta = \frac{1}{N}\sum_{n=0}^{N}(\mathbf{e}(n)) \tag{3.13}$$

where $\mathbf{p}_1(n)$ and $\mathbf{p}_2(n)$ is the position solution sample for the RTK-GPS system and the external navigation system respectfully. N is the total number of samples with $n \in [0, N-1]$ as the counting variable. Adding δ to the external navigation position with the assumption of slow varying bias between the two position solution gives:

$$\mathbf{p}_2(t) + \delta \rightarrow \mathbf{p}_1(t) \tag{3.14}$$

where $\mathbf{p}_1(n)$ and $\mathbf{p}_2(n)$ is the current position solution for the RTK-GPS system and the external navigation system respectfully. The short loss RTK-GPS compensator will trigger if there is a delay in the RTK-GPS system, or a temporary drop out occur. The output frequency of the short loss compensator is set to be the same as the RTK-GPS system, which is estimate by comparing the time each RTK-GPS message is dispatched. This results in prolonging the time where the RTK-GPS is available for the navigation system, and will ensure that the navigation system outputs at a stable frequency. The goal with the compensator is to prevent mission abortion, and make the RTK-GPS system more robust.

3.3 Summary

Chapter 4

Applied software and hardware

4.1 LSTS toolchain

The software that the system is based on was developed by the Underwater Systems and Technology Laboratory (LSTS), which is called the LSTS toolchain [Pinto et al., 2013]. The toolchain was developed for support of networked heterogeneous air and ocean vehicle systems over wireless network. The toolchain contain four different modules, namely Inter-Module Communication (IMC), DUNE, NEPTUS and Glued.

4.1.1 IMC

IMC [Martins et al., 2009] is design to enable interconnections between systems of vehicles, sensors and human operators, which enable the pursuit of common goal by cooperatively exchange real-time information about the environment and updated objectives. The message protocol is oriented around the message, which abstracts hardware and communication heterogeneity with a provided shared set of messages that can be serialized and transferred over different means. The IMC protocol is defined in a single eXtensible Markup Language (XML) document, which simplify the definition of exiting messages and the creation of new messages. A single XML document ease communication between two node when both node use the same document for message definition.

4.1.2 Dune

DUNE (DUNE Uniform Navigation Environment) is a runtime environment for unmanned systems on-board software written in C++. DUNE is capable to interact with sensors, payload and actuators, in addition to communication, navigation, control, manoeuvring, plan execution and vehicle supervision. The software separate operations into different task that each has there own thread of execution. DUNE

apply a message bus that is responsible for forwarding IMC message from the producer to all registered receivers, which is the only way different DUNE tasks is communicating.

A DUNE task is enabled through a configuration file, where the user can choose in which profile the task should be enabled in. The different profiles are used to separate a SIL test from physical testing of the system. The hardware profile configures the system for a hardware setup, while AP-SIl configure DUNE to a software in the loop test. The different profile configuration in DUNE allows for testing the same system used in a hardware setting with a simulator.

4.1.3 Neptus

Neptus is a Command and Control software which is used to command and monitor unmanned systems that is written in Java. Neptus is able to provide coherent visual interface to command despite the heterogeneity in the controlled system that it is interacting with. This allow the operator to command and control unmanned system without the need to dwell into specific command and control software in the unmanned system. The main communication channel for Neptus is IMC, which makes it interoperable with DUNE or other IMC- based peer.

Neptus is able to do MRA (Mission Review and Analysis) after a mission is finished. In the MRA phase Neptus analyse the IMC logs that is collected by e.g. DUNE, such that the result from a completed mission can be presented. In addition Neptus mission review is able to create output files of the log that can be analysed in third party software like Matlab.

4.1.4 Glued

Glued is a minimal Linux operating system distribution, and design with embedded system in mind. It is platform independent, easy to configure and contain only the necessary packages to run on a embedded system. This makes GLUED a light and fast distribution, which is ideal for a on-board operating system for a unmanned system where payload size is normally limited. GLUED is configured through a single configuration file that which can be created for a specific system. A advantage with Glued is that it can be cross-compiled, which allows for compilation of software before it's transferred to the embedded computer.

4.2 RTKLIB

Real-Time Kinematic Library (RTKLIB)[Takasu and Yasuda, 2009] is a open source program package for standard and precise positioning with GNSS developed by T. Takasu. Real-Time Kinematic Library (RTKLIB) can be configured to apply

RTK-GPS, such that raw GNSS data is used estimate the relative position of the rover with respect to the base station in real time. Figure 4.1 shows how RTKLIB can be used in a RTK-GPS mode, where the two main modules here is str2str and rtkrcv. The version of RTKLIB used in this thesis is RTKLIB2.4.2 [RTKLIB].

Rtklib is configured as a moving baseline, where the baseline between the base station and the rover is accurately estimated with centimeter level accuracy. However the concept of moving baseline indicates that the base station is allowed to move, which require continues calculation of the base station position as a standalone GPS. Therefore the error sources that are mitigated in the RTK-GPS solution is present in the GPS position of the base station. The moving baseline configuration is used since a fixed base station location is not known, and a navigation system that should be used at sea will not have a fixed base station location present.

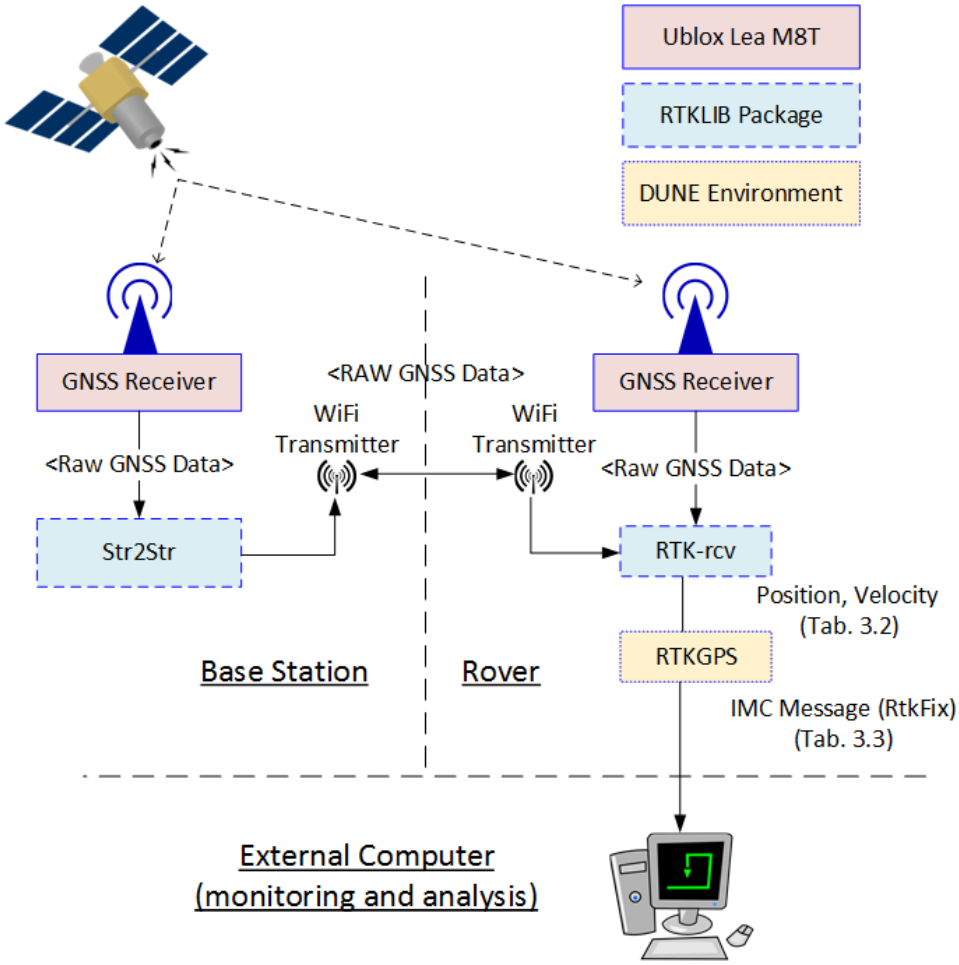

Figure 4.1: The communication structure of RTKLIB

4.3 Pixhawk

3DR Pixhawk is a high-performance autopilot suitable for fixed wing multi rotors, helicopter and other robotic platform that can move. The Pixhawk system comes complete with GPS, imu, airspeed sensor and magnetometer.

4.4 Ardupilot

Ardupilot is an open-source unmanned aerial vehicle platform, able to control fixed wing UAV and multicopters. Ardupilot is used for low level control of the UAV, and is the software that runs on the Pixhawk. Ardupilot is able to communicate to third

party software e.g Dune. Ardupilot uses the sensors in the Pixhawk to calculate the position, velocity and attitude of the UAV, which is sent to DUNE.

4.5 JSBsim

JSBSim [Berndt, 2004] is an open-source flight dynamic model that is able to simulate a physical model of an arbitrary aircraft without the need of specific compiled and linked program code. The simulator is design such that a third party software e.g. Ardupilot can expose the model to external forces and moments. This enable Software In the Loop (SIL) testing of system that is able to run in a hardware configuration with only minor configuration alteration. The physical model that was used in this thesis was developed in the master thesis [Gryte, 2015].

4.6 X8 and nest payload

The Skywalker X8 is fixed wing UAV in a flying wing configuration, which indicate that the UAV has no tail and clear distinction between the wings and fuselage. The X8 is a popular choice for experimental missions at the UAV-lab at the Deparment of Engineering Cybernetic since it's durable, cheap and enough space to carry experimental payload. The X8 is used to test the landing path discussed in this thesis, however the navigation system has been tested in both the X8 and a multicopter system.

The hardware configuration used in the X8 and nest systems is based on the proposed hardware in the paper [Zolich et al., 2015]. The X8 and the nest systems are installed with a BeagleBone embedded computer with the Glued operating system, which is used to run the Dune system, as well as rtklib. The autopilot used in the X8 is a 3DR Pixhawk with ArduPilot ArduPlane software. For the RTK-GPS system Ublox Lea M8T GNSS receivers [U-blox, a,b] are connected to the BeagleBone with uart cable, which is configured with a output rate of 10Hz. The antenna used in the X8 is a Maxtena M1227HCT-A-SMA L1/L2 GPS-GLONASS Active Antenna [Maxtena], and the antenna used in the base station is a Novatel GPS-701-GG [Novatel].

The communication between the X8 and the nest systems is done with Ubiquiti M5 rocket [roc] radios, where the communication between each unit can be done with TCP/UDP/IP.

Chapter 5

Implementation

The landing path generator and the navigation state control system is implememented in the DUNE environment, while controlled and monitored through Neptus. A simplified structure of the autonomous landing system is shown in figure 5.1. The DUNE task Ardupilot is used as the interface for the Ardupilot in the Pixhawk.

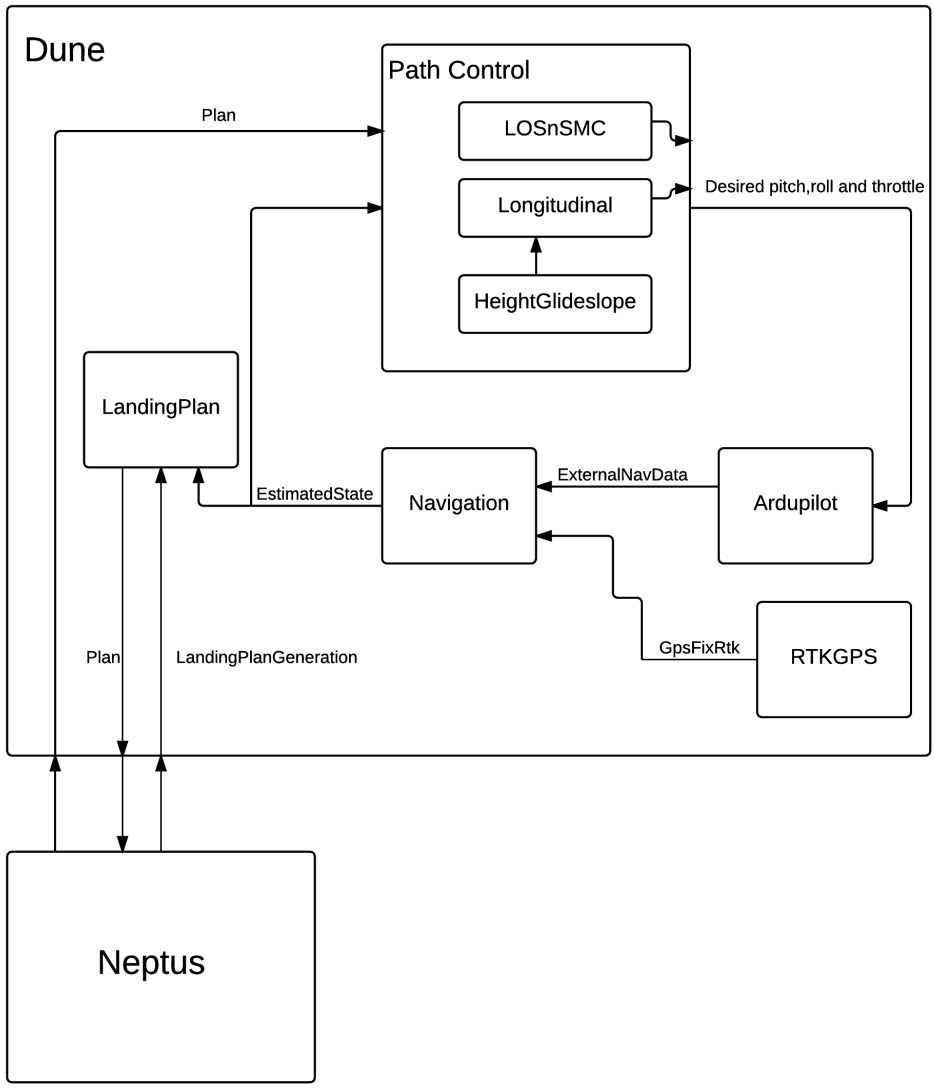

Figure 5.1: A simplified figure of the Dune auto land system

5.1 Landing plan generator

The landing plan generator is implemented to be triggered on the consumption of a LandingPlanGeneration IMC message, which act as the API for the task.

The landing path system is implemented in the DUNE task LandingPlan, which

is design to start generation of a approach and landing path when receiving the IMC message LandingPlanGeneration. The IMC message was created to structure the parameter needed to construct a flyable approach and landing path. As part of the IMC message is the ability to specify the rotation direction of the start and finish circle, as well as if there should be a loiter point in the end of the approach path. The ability to specify the rotation direction of the start and final turning circles ensures that the path can be created to take into account environmental obstacles or wind directions. However if all four variants of the approach path is valid, then the shortest path can be chosen by setting the "Automatic" parameter in the LandingPlanGeneration message true.

The ability to have a loiter manoeuvre at the end of the approach path gives flexibillity when performing a net landing. It allows for final checks of the net condition, or can be used in a dynamic landing operation where the net not stationary e.q. placed on a ship or carried by multi-copters. When configuration the LandingPlan task to perform a dynamical landing only the approach path is created. This was found out to be a preferable solution since a dynamical landing require a feedback loop to correct the desired path, which is currently not included in the landing path system. A solution for performing a dynamical landing is currently research by fellow Master students where the multi-copters is used to catch the UAV, where this landing system is used to create a approach path to ready the UAV for a dynamic landing.

The approach path is created as a FollowPath manoeuvre, which is a manoeuvre with a reference position and offset points that displaced relative to the reference position. The distance between each offset point in each arc is given as a task configuration parameter named "Distance Between Arc Segments"

5.1.1 Landing plan generation API

Parameter name	Description
Automatic (boolean)	If true a standard path where the shortest Dubins path is chosen. Otherwise a user specific path is chosen
Start circle turning counter clockwise (boolean)	If true the start arc is created such that the turning direction is counter clockwise. Otherwise clockwise. Require Automatic==false
Finish circle turning counter clockwise (boolean)	If true the finish arc is created such that the turning direction is counter clockwise. Otherwise clockwise. Require Automatic==false
Wait at loiter (boolean)	If true a unlimited loiter is included in the path before the path continue with the path along the virtual runway.

Table 5.1: Landing path behaviour setting in LandingPlanGeneration

Neptus plug-in

From Neptus the plug-in LandmapLayer, which is an altered version of Neptus plug-in developed in thesis [Frølich, 2015]. Alteration in the plug-in include new parameters, the inclusion of the IMC message LandingPlangeneration and the ability to manually write the global position coordinates of the net.

5.1.2 Approach path

The approach is implemented as a Dubins path from the initial position of the fixed wing UAV to **WP1**. The approach path creation is started when the landing plan generator receive a LandingPlanGeneration message, which trigger the content extraction of the message. The option for the user to specify the rotation direction of the approach path dictates the system flow

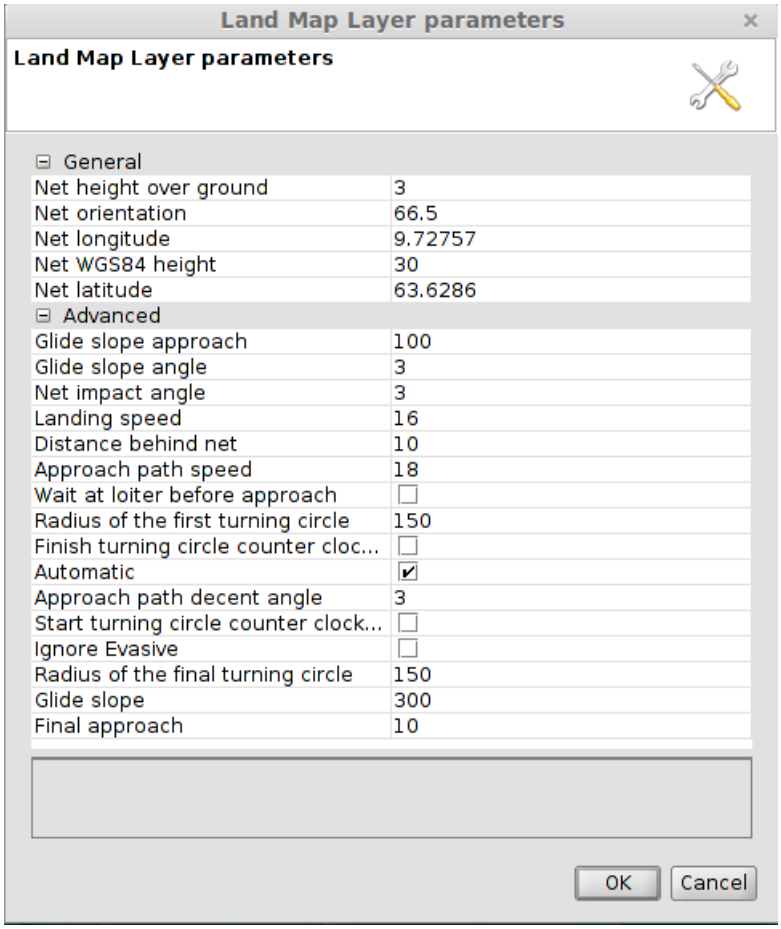

Figure 5.2: Interaction with the landing plan API through Neptus

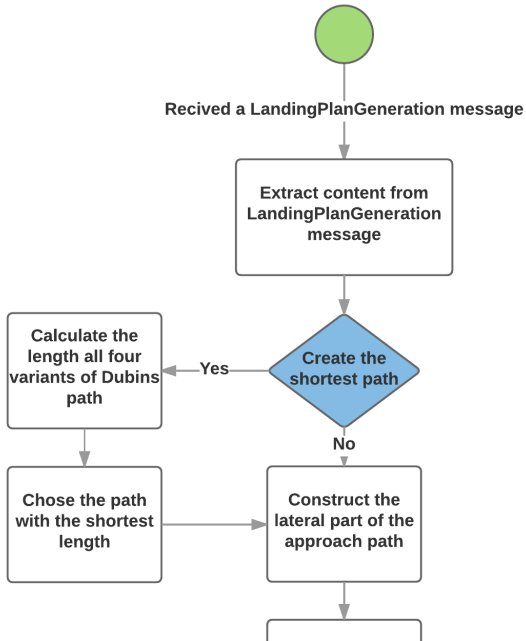

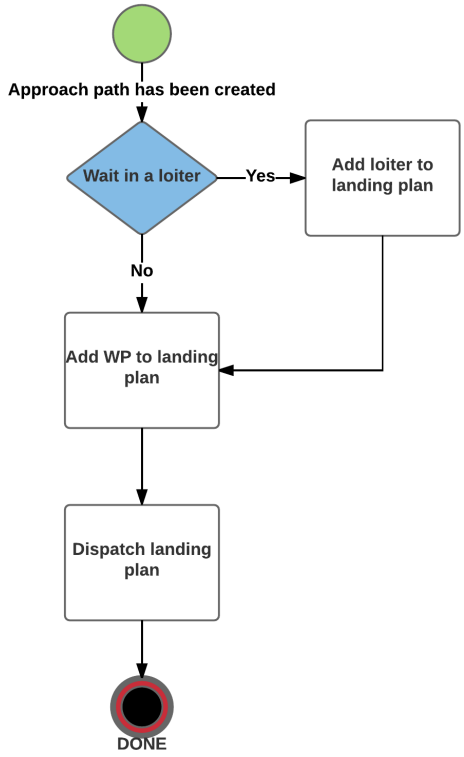

Figure 5.4: Flow chart of the landing plan generation

5.1.3 Landing path

The landing path consist of goto manoeuvres, where the position of the goto manoeuvre is given by the way-points **WP4-2** defined in 3.1.1 relative to the position of the net. Figure 5.4 shown the system flow when a landing path is created in the landing plan generator. A option for the landing path is that it includes a loiter manoeuvre at the beginning, which is defined as a circular manoeuvre around a fixed position with a constant radius. The loiter manoeuvre increase the flexibility of the autonomous landing system, by introducing a manoeuvre that in which the UAV can wait for the landing zone to be prepared. In the case of a dynamic net landing the loiter manoeuvre can be used as a waiting manoeuvre as a final check before the UAV starts to track the position of the net. An other possible application is to apply the loiter manoeuvre in a net landing where the net is carried by multi-copter UAVs, where the copters can wait on the ground until the fixed wing UAV enters the loiter manoeuvre.

5.1.4 Software in the loop simulation

The landing plan was tested in a Software In the Loop (SIL) simulation, where the landing plan generation code runs as if it's connected to the actual hardware. The SIL simulation is used to verify that the code function as it's design to do. During a SIL simulation Ardupilot enters a simulation mode, where the JSBSim simulation is used as replacement of the actual X8 fixed wing UAV. The result obtain from the simulation can be used as a ideal test can of which the performance during a real flight can be compeered against. However the current model of X8 used in the simulation has not been completely verified, such that model error is expected.

A landing path was created to simulate a real landing, where the lateral path is shown in figure 5.5 and the height versus the desired height is shown in figure 5.6. The plan is designed to fit a operational area where the UAV will be within the line of sight of the pilot at any time during execution of the landing plan.

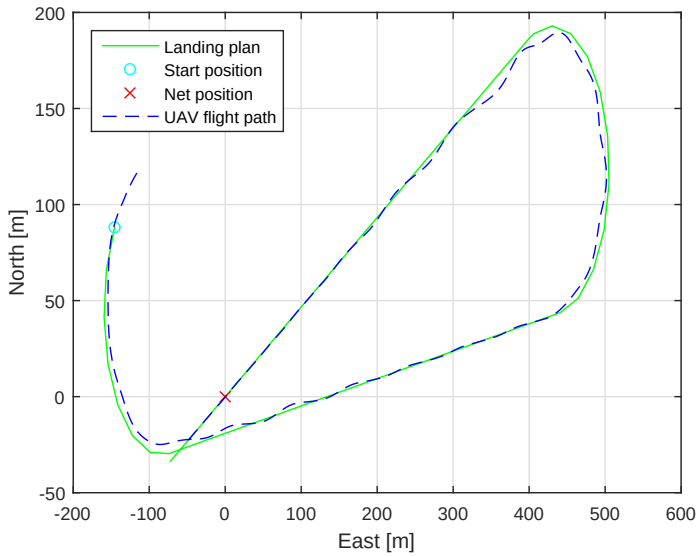

Figure 5.5: North-East plot of a SIL simulation of the autonomous landing system.

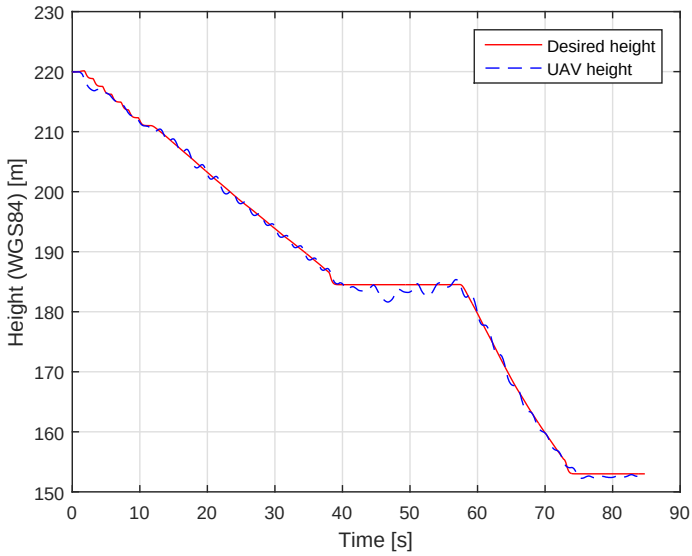

Figure 5.6: The desired height and UAV height when executing the landing plan.

In the case where at the end of the approach path the height does not match the start height of the landing path a downwards spiral is created in order to reach the correct height.

In figure 5.7 the spiral function of the lateral path was tested, with the resulting height profile in figure 5.8. The simulation was performed with a wind disturbance of $9m/s$ from west, in order to observe how the UAV would behave during a simulated landing plan with wind disturbance. The lateral guidance system struggles when flying with the wind, however when flying against the wind it's able to stay on the straight line between the way-points. During the turn in the spiral the lateral guidance system is unable to stay on the circle, thus overshooting the desired path. The longitudinal guidance and control system behave similar to the simulation without wind. This indicate that during a actual flight the wind will affect the error in the longitudinal guidance and control system less then the lateral control and guidance system.

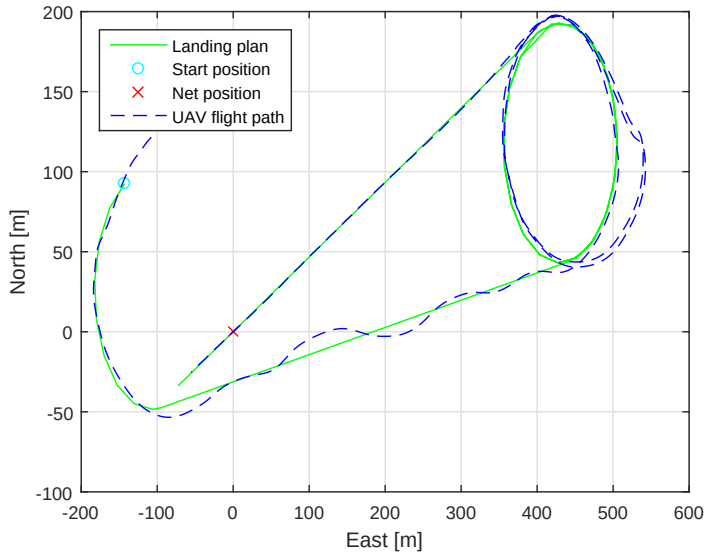

Figure 5.7: North-East plot where the approach path enters a spiral in order to find a path to the correct height. The simulation was performed with $9m/s$ wind from west

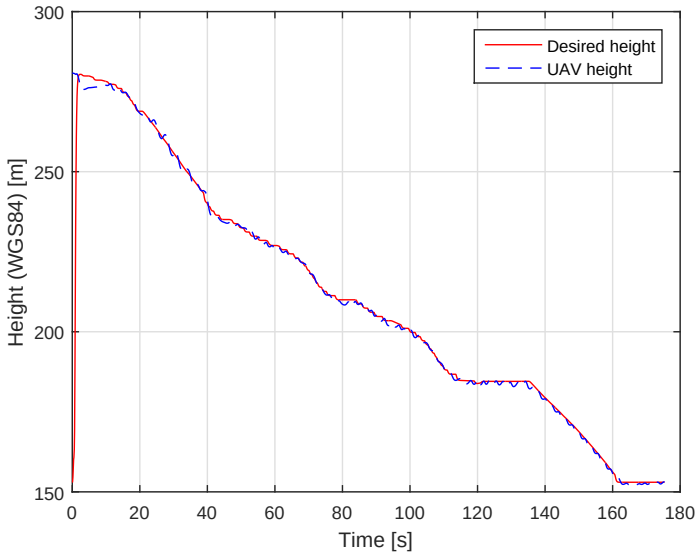

Figure 5.8: The desired height and UAV height when executing the landing plan from a height that trigger a spiral path towards the correct height with maximum decent angle $\gamma_{d_{Max}}$. The simulation was performed with $9m/s$ wind from west

Result of simulations

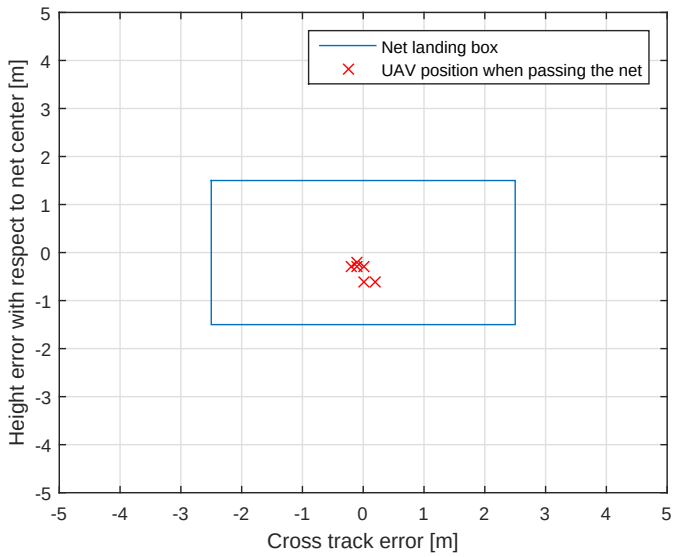

Figure 5.9: UAV position at time of net passing during SIL simulation.

Nr.	Average height error [m]	Average cross track error [m]
1	−0.3	−3.1
2	0.7	−4.0
3	0.2	−3.3
4	0.5	−1.2
5	0.4	−2.5
6	0.2	0.3

5.2 Navigation system

The navigation system is control by a state machine 3.2.2, which is used to control the content of the output IMC messages EstimatedState and NavSources. Depending on which state the navigation system is in the IMC EstimatedState message will either have position solution form the RTK-GPS system or the external navigation system. During a short loss of the RTK the external navigation position is compensated with the average difference between the RTK solution and the external navigation solution.

5.2.1 RTK-GPS system

The RTK-GPS solution is dispatched from the DUNE task RTKGPS, however before the message is accepted by the Navigation task the message must include a valid base station position. The base station position is not included in the output message from RTKlib, which demand the base station position to be calculated locally at the base station as a standalone GNSS receiver. For this purpose the DUNE task BasestationFix is used to lock the current position of the base station, which result in the base station position being transmitted to the RTKGPS task. The navigation system require to now the reference position of the base station in order to use the RTK-GPS solution. However the base station position is currently not part of the output message from rtkrcv. This is resolved by allowing the base station to calculate it's own position as a standalone GPS. The GPS position is transmitted to a local Dune task on the base station, where the operator can decide when the base station can be considered as fixed. When the base station is considered fixed the position is sent to the X8, where it's included in the RTK-GPS solution message.

5.2.2 State machine

Nest system

A nest system is a stationary unit with the sole purpose of providing it's position to the rest of the Dune System. As part of the navigation system the base station

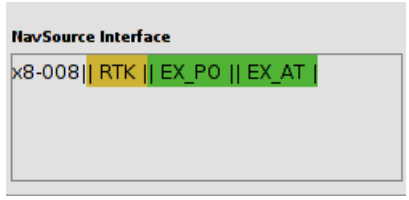

Figure 5.10: Navigation source interface

is defined as a nest, where the GPS position is sent to the RTK-GPS system when fixed. An other nest has been created to obtain the GPS position of the stationary net. The net nest is configured as a rover in RTK-GPS configuration, such that the position relative to the base station is in the same frame as the X8.

5.2.3 Operator interface

The state of the navigation system is monitored though a interface in Neptus. The interface indicate which source the Dune system is using for state information. The interfaced apply a color code to indicate which source is currently in use in addition to all sensor system that are available, as seen in table 5.2.

Color	Description
White	Not available
Yellow	Available, but not in use
Green	Available, and in use

Table 5.2: Net approach parameters

5.3 Summary

Chapter 6

Experimental field tests

The autonomous landing system has successfully been tested in the field, where the result from two subsequent days is presented. The landing plan that was test was only with a virtual net that was placed 26 meters above the ground, using guidance and high level control systems in DUNE. The navigation system used RTK-GPS with the compensator system enabled, which ensures that the positioning of the UAV can be assumed highly accurate. The result of the navigation system is presented in section 6.2.

6.1 Landing system

The wind condition the first day had an windspeed at $8 - 9m/s$ from west, and the second day was calm wind conditions at $1m/s$ from west. Hence the performance of system was tested with two different wind condition, where one strained the performance of the system while the other could be considered as ideal conditions. The criteria used to indicate if the X8 would have hit the net is given in table 6.1, which is related to a net with the dimensions 3 meter height and 5 meter width. The virtual net was placed above a runway at Agdenes, such that the landing path is similar to a landing path where a physical net is used. All landing plan was generated when the UAV was in a loiter manoeuvre, such that the plan could be reviewed and the correct controllers assigned to the plan.

Height acceptance	**Cross track error acceptance**
± 1.5	± 2.5

Table 6.1: Net hit acceptance criteria

6.1.1 Day 1

The first plan created had the approach path cross the landing path, which lead the UAV into the crosswind on the straight line between the circles. This strained the lateral controller introduces oscillatory motion in the UAV. Figure 6.1 shows the lateral landing plan, including the flight path of the UAV and the position of the virtual net. Figure 6.2 shows the desired height and the UAV height during the landing plan.

The behaviour of the lateral path shown in figure 6.1 indicates that the lateral guidance system is struggling to stay on the straight lines in the plan when flying in the crosswind. The oscillatory behaviour affect the path of the UAV when entering the final turning circle, where it overshoot the path. The overshot may cause the UAV to leave the line of sight of the pilot, which is a critical failure in a LOS flight operation. When entering the landing path the UAV continues to oscillate along the final straight line path, all though the UAV was able to have a cross track error at the time of passing the virtual net lower then the cross track error acceptance. The behaviour of the lateral behaviour can be increased by changing the rotation direction of the first turning circle, such that the straight line path between the circle do not cross the landing path. This will also allow the UAV to enter the final turning circle at a better angle. The lookahead distance of the lateral controller can be reduced such that it will react more aggressive when flying in the head wind.

The longitudinal guidance system is able to follow it's reference, all though it is also struggling when attempting a glide slope decent in the head wind. However it should be noted that the path shown in figure 6.2 was constructed with a net impact angle of $\gamma_n = 3\,\text{deg}$, which resulted in the desired height failure to converge to the path due the smoothing filter introducing a constant bias from the desired path. In order for the desired height from the longitudinal guidance system to converge to the desired path the net impact angle γ_n was set to zero. However this affect the total altitude descent along the landing path since now only the glide slope is used to reduce the altitude of the UAV.

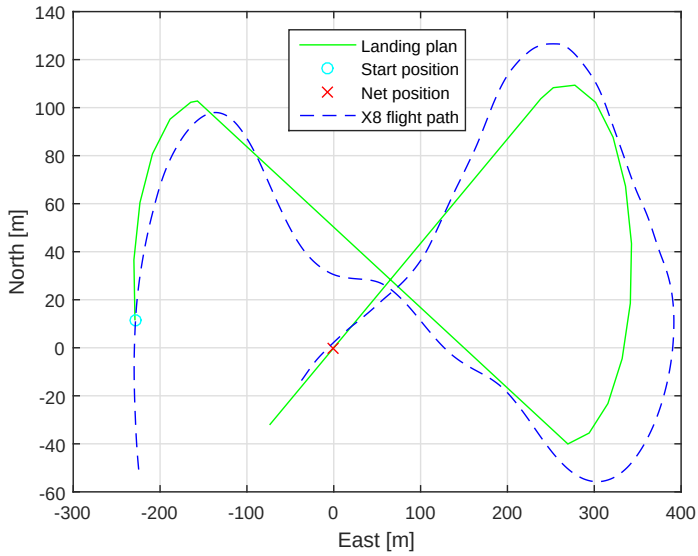

Figure 6.1: North-East plot of a landing plan

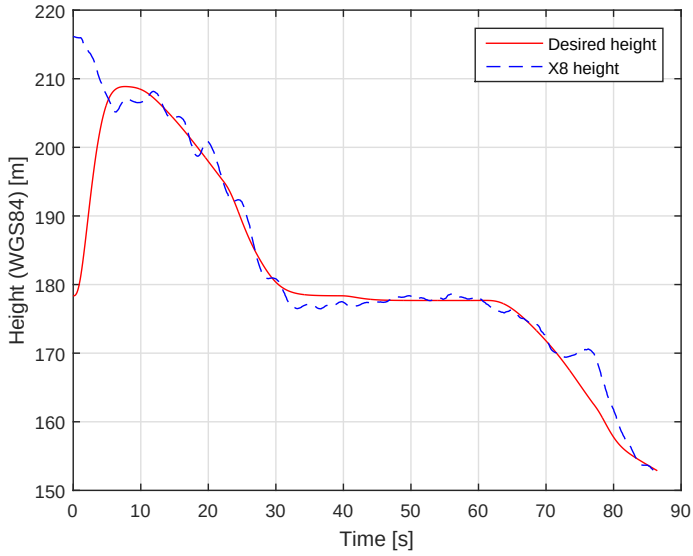

Figure 6.2: Height profile of landing plan with 3 deg net impact angle

A new landing plan, where the desired height and UAV during the landing plan

is shown in figure 6.3, was generated with the net impact angle $\gamma_n = 0$. The effect of setting the net impact angle to zero gave a better performance from the height guidance system. At the time the UAV passed the virtual net the hight error with respect the height of the net center was within the height error acceptance.

The minimum altitude that was used at the start of the landing path was set to $56m$ above the runway. This is due to the length restriction of both the airfield and the operational area where the UAV is visible for the pilot. With the current landing plan and a landing direction from east the minimum height at which the UAV can starts its landing path is set to $56m$ above ground. The effect of this requirement is discussed further in section 6.1.1.

During the new path the UAV was able to stay on the straight line towards the net. However the UAV still have oscillatory behaviour along the straight line connecting the two circles, with a large overshoot in the final turn. A better path would be to avoid flying in the cross wind as much as possible, which would result in a smoother path between the circles. However this will not remove the overshot in the final turn, all thought it will be reduced since the UAV is not in a oscillatory motion when entering the final circle.

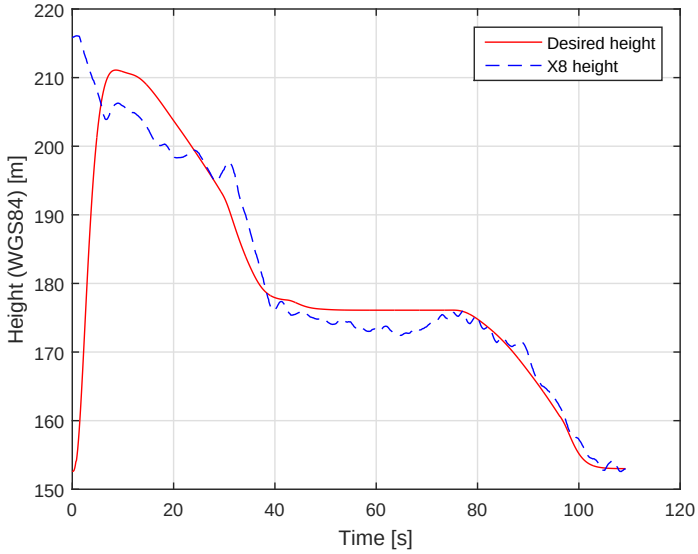

Figure 6.3: Height profile of landing plan with 0 deg net impact angle

In order to reduce the oscillatory motion of the UAV a new path was constructed where the rotation direction of the first circle was changed to counter clockwise, as

shown in figure 6.4. The new path had its straight line path between the circles parallel to the wind direction, which resulted in less oscillatory motion and a smaller entry tangential angle into the final turning circle. However the overshoot in the final circle is still present, and is a result of the UAV attempting to turn up against the wind. The oscillatory motion was reduced by changing the rotation direction of the first turning circle, however the UAV is still not able to stay on the straight line paths in the landing plan.

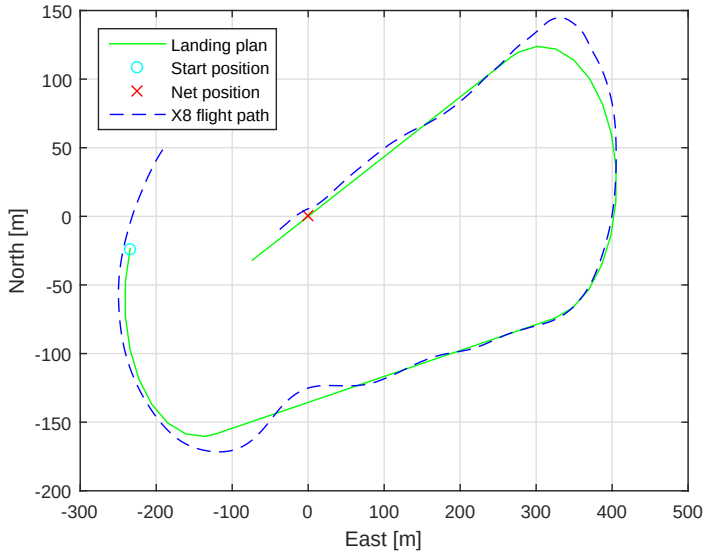

Figure 6.4: North-East plot where the straight line segment between the two circles give a path parallel to the wind

In order to further reduce the oscillatory motion of the lateral controller the lookahead distance was reduced to make the controller more aggressive towards the wind. The effect of this change is shown in figure 6.5, where the oscillatory motion is almost completely removed. However the overshot at end of the final circle indicates that the lateral controller is struggling to handle a turning circle.

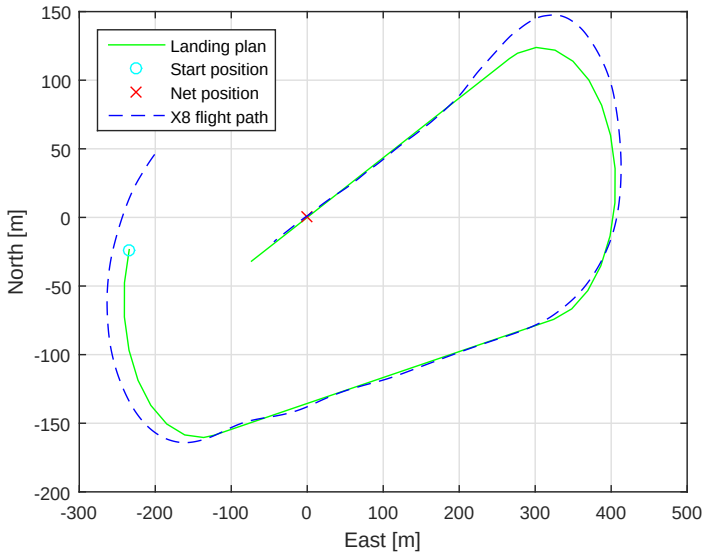

Figure 6.5: North-East plot where the lookahead distance of the lateral controller was reduced to increase performance when flying against the wind

Looking at the desired roll (ϕ_d) and the actual roll (ϕ) of the UAV at the time of the final turn, shown in figure 6.6, it's observed that the controller does not try to keep a constant bank through the turn. Instead it lowering the roll angle, which in turn affect the performance of the UAV at the end of the turn. The performance might be reduced by reducing the distance between each arc segments in the turning circle, and experimenting with the radius of the turning circle. However this was not attempt during the first day, all thought attempts to reduce overshot by lowering the distance between each arc segments was performed the following day.

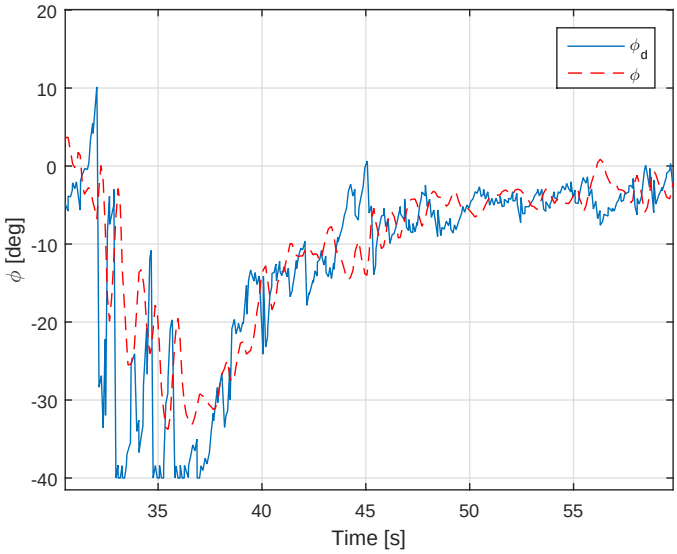

Figure 6.6: The desired roll and actual roll of the UAV

Summary of day 1

The result from the first day was affected with strong wind condition, in which the UAV struggled to stay on the path. The mean height and cross track error is listed in table 6.2, where the first column indicate the number of the landing attempt. As seen in table 6.2 the average cross track error equals to $5.4m$

Nr.	**Average height error [m]**	**Average cross track error [m]**
1	1.5	6.1
2	2.6	6.7
3	0.9	5.5
4	0.1	2.8
5	1.7	2.0
6	1.3	6.8
7	1, 8	9.1
8	1.2	8.2
9	1.9	5.9
10	1.5	4.4
11	1.5	1.4
Average	1.5	5.4

Table 6.2: Mean height and cross track error from day 1

The longitudinal guidance system was able to keep a stable average height error during the landing plans. However the longitudinal control system must be further fine tuned in order to achieve the precision needed to perform a autonomous landing during windy conditions. A table containing if a landing plan would result in a net landing is presented in table 6.3. The success rate of the first day gives a 36.3% probability of successfully landing in the net, which indicate that alteration to the current landing system is needed in order to achieve better performance in strong wind conditions.

Nr.	**Height error [m]**	**Cross track error [m]**	**Height acceptance**	**Cross track error acceptance**	**Net hit**
1	2.8	2.1	X	OK	X
2	2.7	−4.5	X	X	X
3	0.9	−1.6	OK	OK	OK
4	0.0	5.4	OK	X	X
5	0.8	5.3	OK	X	X
6	2.1	−1.6	X	OK	X
7	0.7	2.3	OK	OK	OK
8	−1.5	−5.4	X	X	X
9	1.9	0.8	X	OK	X
10	0.3	1.1	OK	OK	OK
11	−1.3	0.2	OK	OK	OK

Table 6.3: Table containing the result of each landing attempt

The content of table 6.3 is shown in figure 6.7, where the net is marked as a whole line and all landing attempts are marked as crosses. The osilatory motion in the lateral plane by the UAV is reflected in the placement of the crosses. However the placement of the cross is evenly divided along the cross track error axis, which is not reflected in the placement along the height error axis. The placement along the height error axis indicates that the UAV

Net offset [m]	**Needed decent height [m]**	**Glide slope length [m]**	**Glide slope angle** [deg]
0	56	700	4.6
3	53	700	4.3
3	53	300	9.5

Table 6.4: Different decent heights and length of glide slope with responding glide slope angle

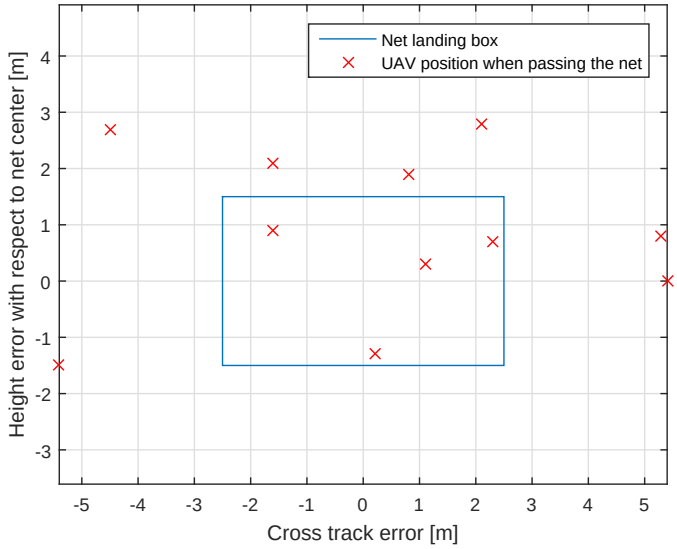

Figure 6.7: Position of UAV relative to the net center at the time of net passing

The maximum length of the landing path with the radius of the final turning circle must be within the flight operation area. On Agdenes when attempting to land from the East the restriction is estimated to be $700m$, with minimum altitude of $56m$. The minimum altitude will vary if the UAV can start its landing path from the west, however this will only be the case during calm wind condition or a wind direction from the east. In addition increased glide slope angle will result in the UAV to build up speed, however decreasing the throttle in order to reduce lift might be a method used to quickly lose hight during the landing path.

6.1.2 Day 2

The second day had calm wind condition, which is considered as ideal field test conditions for the autonomous landing system. For the new landing plan the virtual net was moved in order for the landing path to use more of the runway. In addition the heading of the net was changed such the landing path became parallel to the runway. The main goal with the flight today was to reduce to overshot in the final turn, and to investigate how to increase the performance of the height guidance system. To increase the height difference between the net center and the start of the landing path both the length of the glide slope and glide slope angle was increased.

The path generated with the new parameters is shown in figure 6.8. The lateral path overshoots in both the start and final turning circles. As seen in figure 6.9 the roll motion of the UAV does not follow the desired roll, which is due to the low level roll controller is tuned for manual flight where rapid changes in the actuators is undesired. In addition the control surface used to control the roll of the UAV is also used to control the pitch, which results in having to weight the performance in heading against the ability to follow a height reference.

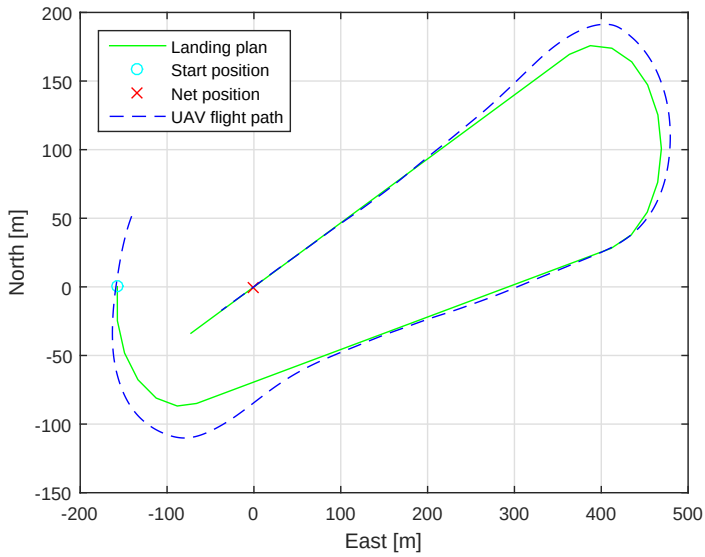

Figure 6.8: North-East plot

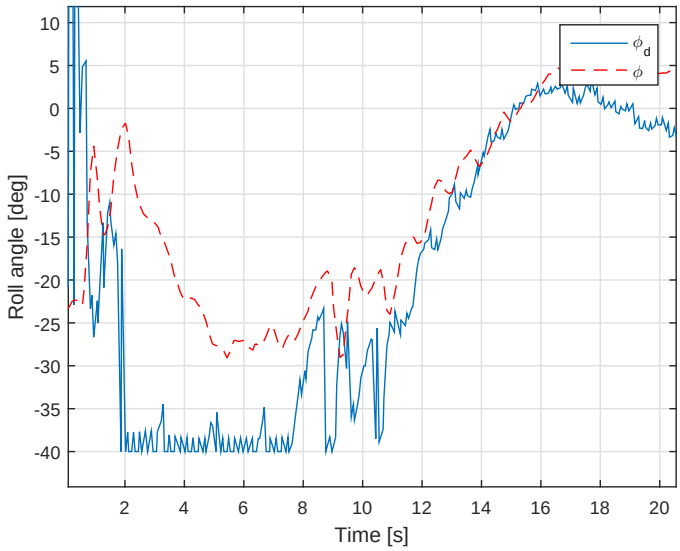

Figure 6.9: Roll

The resulting desired height and UAV height from the new path, shown in figure 6.10, shows that the UAV was unable to follow a glide slope with glide slope angle $\gamma_l = 8\,\text{deg}$. A major reason for this behaviour is due to the failure of the UAV pitch to follow the desired pitch, as shown in figure 6.11. The pitch appear to to saturated in the low level controller since it does not reach the desired pitch. Better tuning of the low level control system might reduce the bias and lag between actual and desired pitch value, however the reason for the saturation must be further investigated. A restriction in the desired pitch available for the control system, indicate that a new strategy is need in a autonomous landing system where speed assignment during the landing path must be investigated.

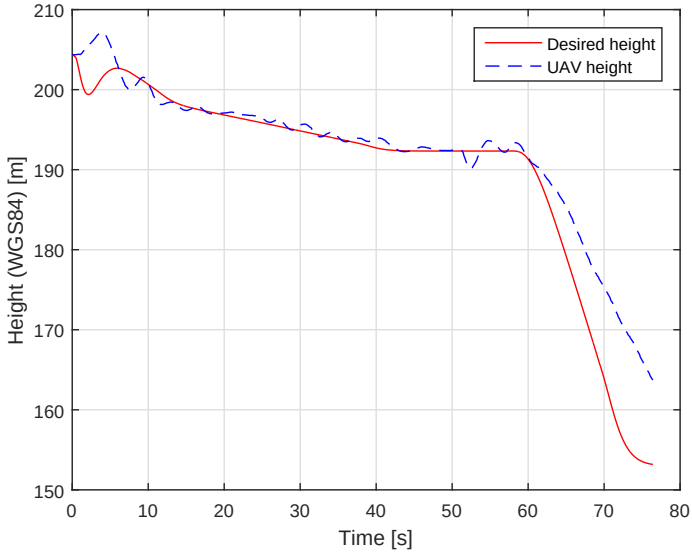

Figure 6.10: Height

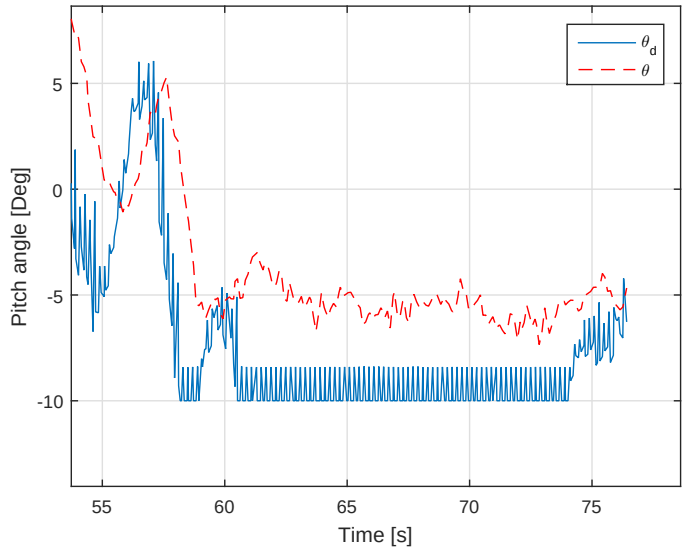

Figure 6.11: Pitch

In order to reduce the overshot in the final turning circle the distance between

each arc segments each turning circle was reduced. The goal for with this alteration was to get the lateral controller to keep the roll angle in order to increase the turning performance. Figure 6.12 shows the the resulting path when the arc segment distance is reduced. The overshot in the final turning circle is reduced, and the cross track error in the final turning circle is shown in figure 6.13 indicates that the performance of the UAV increase with short distance between arc segments. A long term solution for reducing overshot in a turning circle would be a dedicated controller for turning manoeuvre. If combined with the current lateral controller which is designed to stay on a straight line between way-point the result will be a controller that is well suited for performing a autonomous landing.

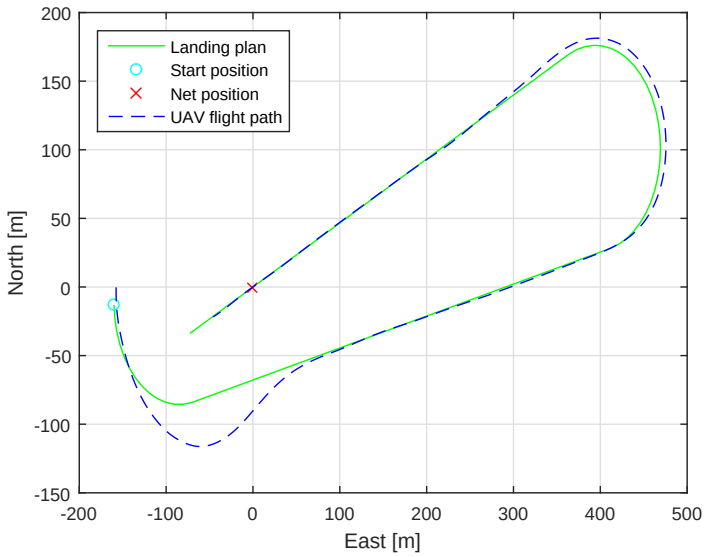

Figure 6.12: North-East plot where the distance between each arc segments has been reduced from $25m$ to $10m$

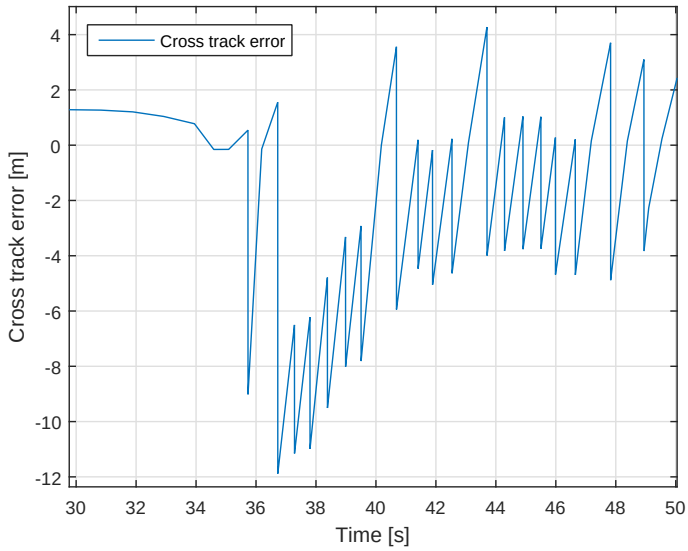

Figure 6.13: Cross track error in the final turning circle

Summary day 2

The second day had more experimental testing then the first day, where the limits of the height profile and reducing the overshoot in the final turning circle was the main focus. The testing of limits for glide slope angle is reflected in table 6.6 where the net misses is due to height error. With the current system the limit was found to be $\gamma_l = 6\,\text{deg}$, however better tuning of low level pitch controller and reducing landing speed could increase the limitation on the glide slope angle. The short final approach length resulted in the UAV to have a short distance of which the net center height could be reached. A longer final approach would result in a higher success rate, however this would require either a longer landing path or shorter glide slope. The final approach could be increased to $120m$ by moving the net further west over. The risk with a large final approach during a autonomous landing in a real net would be the prolonged time the UAV flies $3 - 4m$ above ground. A loss of high accurate positioning system could then result in a crash.

Nr.	Height error [m]	Cross track error [m]	Height acceptance	Cross track error acceptance	Net hit
1	14.4	0.1	X	OK	X
2	1.3	0.6	OK	OK	OK
3	1.1	−0.2	OK	OK	OK
4	1.4	0.1	OK	OK	OK
5	1.1	0.1	OK	OK	OK
6	2.0	−0.2	X	OK	X
7	2.3	0.2	X	OK	X
8	7.0	0.3	X	OK	X

Table 6.5: Table containing the result of each landing attempt

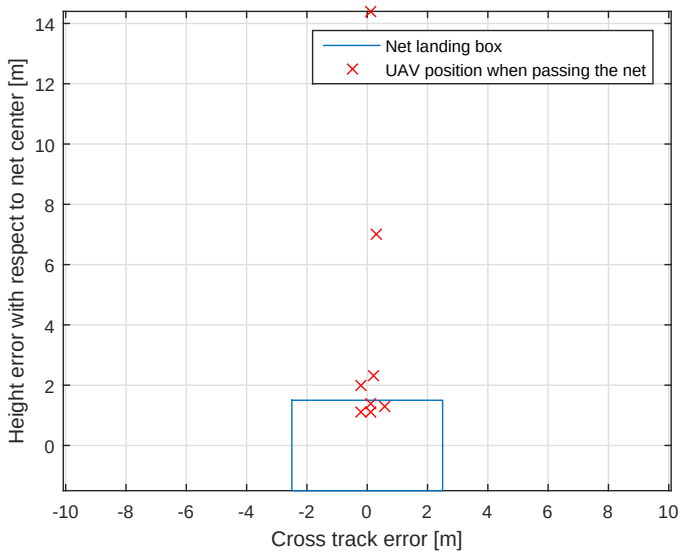

Figure 6.14: Position of the UAV relative to the net center at the time of net passing

The performance of the lateral controller increase during calm wind condition, however the performance of the longitudinal controller is the same as during windy conditions. Table 6.6 list up the average height error and cross track error relative to the desired height and path.

Nr.	Average height error [m]	Average cross track error [m]
1	2.2	3.8
2	1.2	3.4
3	0.9	−1.8
4	2.5	−0.2
5	3.0	0.3
6	1.6	0.2
7	1, 9	−2.3
8	1.9	−0.1

Table 6.6: Average height and cross track error from day 2

6.2 Navigation

The testing of the navigation system is restricted to the X8, however the same navigation system was used in a multicoper UAV both days.

6.2.1 RTK-GNSS performance

The performance of the RTK-GNSS system during the first day of executing landing plans is summaries in table 6.7, which shows that RTK-GNSS kept a stable FIX during the landing plan experiment. The same result was achieved during the second day during the execution of the landing plans, however the RTK-GPS experienced problem later the second day, due to lost contact with the base station. The expected reason is that pore satellite geometry made effective use of RTK-GPS difficult.

Nr.	FIX %	FLOAT %	NONE %
1	99.5	0.5	0.0
2	99.5	0.5	0.0
3	99.8	0.0	0.0
4	100	0.0	0.0
5	100	0.0	0.0
6	100	0.0	0.0
7	99.9	0.1	0.0
8	99.7	0.3	0.0
9	99.3	0.7	0.0
10	100	0.0	0.0
11	100	0.0	0.0

Table 6.7: Performance of the RKT-GNSS system the first day during the executing of the landing plans

6.2.2 Short loss compensator

The short loss compensator was designed to prolong the availability of the RTK-GPS, such that a flight plan does not get interrupted due to a temporary problem with the RTK-GNSS. During a flight the second day the glsrtk-gps experienced a short drop out, as seen in figure 6.15. Even though the RTK-GPS position solution is unavailable the navigation system is still able to supply high accurate position solution due to the short RTK-GNSS compensator as seen in figure 6.16. The duration of the short RTK-GPS could be expanded, and currently the time limitation of the compensator where the position solution start to diverge is unknown.

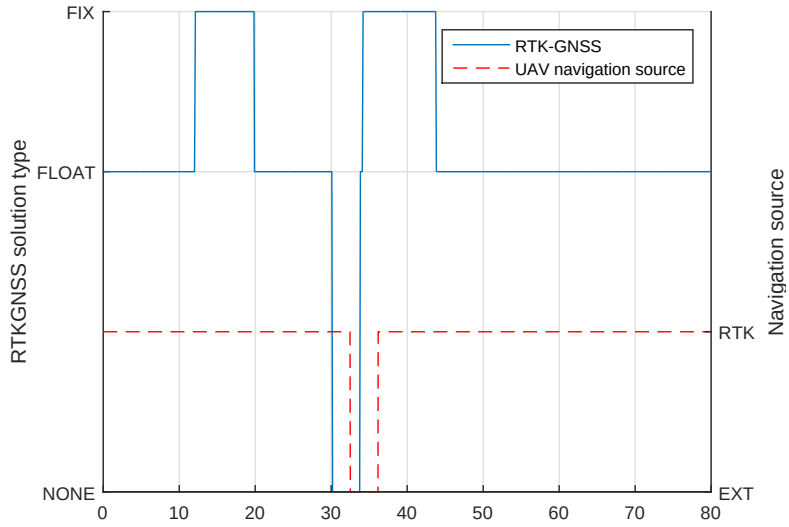

Figure 6.15: State of RTK-GNSS system and UAV navigation source.

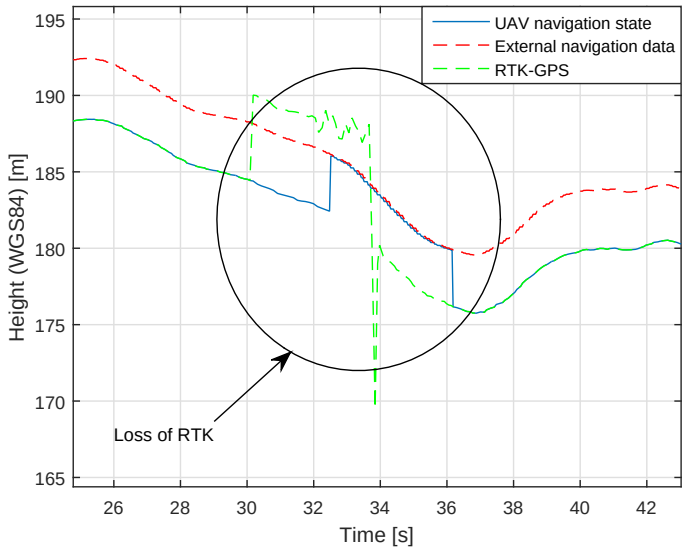

Figure 6.16: Loss of RTK-GPS triggers the short loss compensator such that the UAV keeps the RTK-GPS position solution longer

6.3 Summary

This chapter showed the performance of a X8 fixed wing UAV performing a autonomous landing in a virtual net. The performance of the navigation system is acceptable for a autonomous system by supplying a stable highly accurate position solution, with redundancy for short RTK-GPS loss periods. The landing plan still require further testing to develop path parameters that will result in a successful net landing. The path parameters are depending on the ability for the control system to follow the desired path, which might prove demanding in the longitudinal plane for large change in high over a short distance.

Chapter 7

Conclusion and recommendation for further work

7.1 Conclusion

7.2 Recommendation for further work

References

Ubiquiti networks rocket m powerful 2x2 mimo airmax basestation models: M5, rm5-ti, m3, m365, m2, rm2-ti, m900 datasheet. https://dl.ubnt.com/datasheets/rocketm/RocketM_DS.pdf. Accessed: 16.05.2016.

D Blake Barber, Stephen R Griffiths, Timothy W McLain, and Randal W Beard. Autonomous landing of miniature aerial vehicles. *Journal of Aerospace Computing, Information, and Communication*, 4(5):770–784, 2007.

Brian A Barsky and Tony D DeRose. Geometric continuity of parametric curves: three equivalent characterizations. *IEEE Computer Graphics and Applications*, (6):60–68, 1989.

Randal W Beard and Timothy W McLain. *Small unmanned aircraft: Theory and practice*. Princeton university press, 2012.

Jon S Berndt. Jsbsim: An open source flight dynamics model. In *in C++. AIAA*. Citeseer, 2004.

Lester E Dubins. On curves of minimal length with a constraint on average curvature, and with prescribed initial and terminal positions and tangents. *American Journal of mathematics*, 79(3):497–516, 1957.

Joao Fortuna and Thor I Fossen. Cascaded line-of-sight path-following and sliding mode controllers for fixed-wing uavs. In *Control Applications (CCA), 2015 IEEE Conference on*, pages 798–803. IEEE, 2015.

Thor I Fossen. *Handbook of marine craft hydrodynamics and motion control*. John Wiley & Sons, 2011.

Marcus Frølich. Automatic ship landing system for fixed-wing uav. Master's thesis, Norwegian University of Science and Technology, NTNU, 2015.

Kristoffer Gryte. High angle of attack landing of an unmanned aerial vehicle. Master's thesis, Norwegian University of Science and Technology, NTNU, 2015.

Sungsik Huh and David Hyunchul Shim. A vision-based automatic landing method for fixed-wing uavs. *Journal of Intelligent and Robotic Systems*, 57(1-4): 217–231, 2010.

Insitu. Skyhook universal productcard. https://insitu.com/images/uploads/pdfs/Skyhook_Universal_ProductCard_PR041615.pdf. Accessed: 13.05.2016.

H Jin Kim, Mingu Kim, Hyon Lim, Chulwoo Park, Seungho Yoon, Daewon Lee, Hyunjin Choi, Gyeongtaek Oh, Jongho Park, and Youdan Kim. Fully autonomous vision-based net-recovery landing system for a fixed-wing uav. *Mechatronics, IEEE/ASME Transactions on*, 18(4):1320–1333, 2013.

Ricardo Martins, Paulo Sousa Dias, Eduardo RB Marques, José Pinto, Joao B Sousa, and Femando L Pereira. Imc: A communication protocol for networked vehicles and sensors. In *Oceans 2009-Europe*, pages 1–6. IEEE, 2009.

Maxtena. M1227hct-a-sma l1/l2 gps-glonass active antenna, data sheet. http://www.farnell.com/datasheets/1681376.pdf. Accessed: 18.12.2015.

Pratap Misra and Per Enge. *Global Positioning System: Signals, Measurements and Performance Second Edition*. Lincoln, MA: Ganga-Jamuna Press, 2011.

Novatel. Gps-701-gg and gps-702-gg, data sheet. www.novatel.com/assets/Documents/Papers/GPS701_702GG.pdf. Accessed: 18.12.2015.

Joel Pinto, Paulo S Dias, Rui P Martins, Joao Fortuna, Eduardo Marques, and Joao Sousa. The lsts toolchain for networked vehicle systems. In *OCEANS-Bergen, 2013 MTS/IEEE*, pages 1–9. IEEE, 2013.

RTKLIB. Rtklib ver. 2.4.2 manual. http://www.rtklib.com/prog/manual_2.4.2.pdf. Accessed: 18.12.2015.

Robert Skulstad and Christoffer Lie Syversen. Low-cost instrumentation system for recovery of fixed-wing uav in a net. Master's thesis, Norwegian University of Science and Technology, NTNU, 2014.

Robert Skulstad, Christoffer Lie Syversen, Mariann Merz, Nadezda Sokolova, Thor I Fossen, and Tor A Johansen. Net recovery of uav with single-frequency rtk gps. In *Aerospace Conference, 2015 IEEE*, pages 1–10. IEEE, 2015.

Bjørn Amstrup Spockeli. Integration of rtk gps and imu for accurate uav positioning. Master's thesis, Norwegian University of Science and Technology, NTNU, 2015.

Tomoji Takasu and Akio Yasuda. Development of the low-cost rtk-gps receiver with an open source program package rtklib. In *international symposium on GPS/GNSS*, pages 4–6. International Convention Centre Jeju, Korea, 2009.

Peter JG Teunissen. A new method for fast carrier phase ambiguity estimation. In *Position Location and Navigation Symposium, 1994., IEEE*, pages 562–573. IEEE, 1994.

Peter JG Teunissen. The least-squares ambiguity decorrelation adjustment: a method for fast gps integer ambiguity estimation. *Journal of Geodesy*, 70(1-2): 65–82, 1995.

Antonios Tsourdos, Brian White, and Madhavan Shanmugavel. *Cooperative path planning of unmanned aerial vehicles*, volume 32. John Wiley & Sons, 2010.

U-blox. Neo/lea-m8t u-blox m8 concurrent gnss timing modules, data sheet. https://www.u-blox.com/sites/default/files/NEO-LEA-M8T_DataSheet_(UBX-14006196).pdf, a. Accessed: 18.12.2015.

U-blox. U-blox m8 receiver description including protocol specification. https://www.u-blox.com/sites/default/files/products/documents/u-bloxM8_ReceiverDescrProtSpec_%28UBX-13003221%29_Public.pdf?utm_source=en%2Fimages%2Fdownloads%2FProduct_Docs%2Fu-bloxM8_ReceiverDescriptionProtocolSpec_%28UBX-13003221%29_Public.pdf, b. Accessed: 18.12.2015.

Bjørnar Vik. Integrated satellite and inertial navigation systems. *Department of Engineering Cybernetics, NTNU*, 2014.

Dong Il You, Yeun Deuk Jung, Sung Wook Cho, Hee Min Shin, Sang Hyup Lee, and David Hyunchul Shim. A guidance and control law design for precision automatic take-off and landing of fixed-wing uavs. In *AIAA Guidance, Navigation, and Control Conference*, pages 1–19, 2012.

Artur Zolich, Tor Arne Johansen, Krzysztof Cisek, and Kristian Klausen. Unmanned aerial system architecture for maritime missions. design & hardware description. In *2015 Workshop on Research, Education and Development of Unmanned Aerial Systems (RED-UAS)*, pages 342–350. IEEE, 2015.

Appendix A

Landing plan generation API

The landing plan generation API consist of the IMC LandingPlanGeneration, where the field with description is given in table

Field name	**Type**	**Description**
Command	Enumerated	Command the plan database to generate the plan, with the option of executing the plan after generation.
Operation	Enumerated	Type of operation started.
Plan identifier	Plain text	Plan identifier.
Reference latitude	rad	Reference latitude for the landing path.
Reference longitude	rad	Reference longitude for the landing path.
Reference height	m	Reference height for the landing path.
Height over ground	m	Offset from the reference height to placement.
Reference point heading	rad	Heading of the reference point in NED frame.
Distance behind	m	Aiming point behind the reference point.
Final approach length	m	The length of the final approach towards the reference point.
Final approach angle	rad	The decent angle of the final approach vector.
Glide slope length	m	The length of the glide slope in the landing path.
Glide slope angel	rad	The decent angle of the glide slope.
Approach decent angle	rad	The decent angle of the approach path.
Approach length	m	The length of the vector from the end of the approach path to the glide slope.
Landing speed	m/s	The landing speed.
Approach speed	m/s	The approach speed.
Start turning circle radius	m	The radius of the first turning circle.
Finish turning circle radius	m	The radius of the second turning circle.
Automatic generate landing plan	Flag	The approach path will calculate the shortest path form the initial position towards the start of the landing path.
Start circle turning direction	Flag	Manually setting the rotation direction of the first circle.
Finish circle turning direction	Flag	Manually setting the rotation direction of the finish circle.
Wait at loiter	Flag	Setting if after the approach path the UAV should enter a loiter manoeuvre.

Table A.1: Table containing the landing plan generation API

Appendix B

Guidance and control system

The autonomous landing system is design to be independent from any types of guidance and control system. However this hold only true when the guidance and control system is implemented in the DUNE environment due to the requirement of an accurate navigation system. The control system is separated into two groups, high level and low level control. The low level control is the control loops for the actuators, which are only controlled by ardupilot. The high level controllers depend on the the configuration of Ardupilot, which is listed in table B.1.

B.1 Lateral controller

The lateral controller used in the autonomous landing system is based on the paper [Fortuna and Fossen, 2015], which is a s

Mode	**Description**
Guide	Ardupilot set-point guidance and control system
FBWB	DUNE lateral controller with desired height controlled in a set-point controller in Ardupilot
FBWA	DUNE lateral and longitudianl controller, where control input is sent directly to the low level controllers in Ardupilot

Table B.1: Guidance and control modes in autopilot viable for the landing system

Parameter	Value
Lookahead	50.0
Rho	1.0
Lambda	0.35
Kd	1.5
Bandwidth	3.0
Roll Time Const	0.5
Maximum Bank	40.0

Parameter	Value
Throttle Proportional gain	0.3
Throttle Integrator gain	0.1
Throttle Proportional height gain	0.3
Gamma Proportional gain	1.0
Trim throttle	44.0

Parameter	Value
LOS Proportional gain up	0.9
LOS Integral gain up	0.1
LOS Radius up	14
LOS Proportional gain down	0.9
LOS Integral gain down	0.1
LOS Radius down	14
LOS Proportional gain line	1.0
LOS Integral gain line	0.02
LOS Radius line	25
Time constant refmodelZ	1.0
Time constant refmodelGamma	1.0
Use reference model	True
Height bandwidth	10
Vertical Rate maximum gain	0.3

B.2 Longitudinal controller

The longitudinal controller is based on the paper [You et al., 2012]

Need to refer to the height smoothing filter with advantage and disadvantage.

Appendix C

Navigation performance results

Nr.	FIX %	FLOAT %	NONE %
1	99.2	0.8	0.0
2	100	0.0	0.0
3	99.9	0.1	0.0
4	99.9	0.1	0.0
5	100	0.0	0.0
6	100	0.0	0.0
7	99.6	0.4	0.0
8	99.9	0.31	0.0

Table C.1: Performance of the RKT-GNSS system the first day during the executing of the landing plans

Appendix D

Rtklib Configuration

Configuration of RTKLIB,rtkrcv is given bellow.

```
# RTKNAVI options (2015/10/30 13:05:07, v.2.4.2)

pos1-posmode       =movingbase # (0:single,1:dgps,2:kinematic,
3:static,4:movingbase,
5:fixed,6:ppp-kine,
7:ppp-static)
pos1-frequency     =l1         # (1:l1,2:l1+l2,3:l1+l2+l5,
4:l1+l2+l5+l6,
5:l1+l2+l5+l6+l7)
pos1-soltype       =forward    # (0:forward,1:backward,2:combined)
pos1-elmask        =10         # (deg)
pos1-snrmask_r     =off        # (0:off,1:on)
pos1-snrmask_b     =off        # (0:off,1:on)
pos1-snrmask_L1    =0,0,0,0,0,0,0,0,0
pos1-snrmask_L2    =0,0,0,0,0,0,0,0,0
pos1-snrmask_L5    =0,0,0,0,0,0,0,0,0
pos1-dynamics      =on        # (0:off,1:on)
pos1-tidecorr      =off        # (0:off,1:on,2:otl)
pos1-ionoopt       =brdc       # (0:off,1:brdc,2:sbas,3:dual-freq,
4:est-stec,5:ionex-tec,
6:qzs-brdc,7:qzs-lex,8:vtec_sf,
9:vtec_ef,10:gtec)
pos1-tropopt       =saas       # (0:off,1:saas,2:sbas,3:est-ztd,
4:est-ztdgrad)
pos1-sateph        =brdc       # (0:brdc,1:precise,2:brdc+sbas,
```

```
3:brdc+ssrapc,4:brdc+ssrcom)
pos1-posopt1       =off        # (0:off,1:on)
pos1-posopt2       =off        # (0:off,1:on)
pos1-posopt3       =off        # (0:off,1:on)
pos1-posopt4       =off        # (0:off,1:on)
pos1-posopt5       =off        # (0:off,1:on)
pos1-exclsats      =           # (prn ...)
pos1-navsys        =7          # (1:gps+2:sbas+4:glo+8:gal+16:qzs+32:comp)
pos2-armode        =fix-and-hold # (0:off,1:continuous,2:instantaneous,
3:fix-and-hold)
pos2-gloarmode     =off        # (0:off,1:on,2:autocal)
pos2-bdsarmode     =off        # (0:off,1:on)
pos2-arthres       =3
pos2-arlockcnt     =0
pos2-arelmask      =0          # (deg)
pos2-arminfix      =10
pos2-elmaskhold    =0          # (deg)
pos2-aroutcnt      =5
pos2-maxage        =30         # (s)
pos2-syncsol       =on        # (0:off,1:on)
pos2-slipthres     =0.05       # (m)
pos2-rejionno      =30         # (m)
pos2-rejgdop       =30
pos2-niter         =1
pos2-baselen       =0          # (m)
pos2-basesig       =0          # (m)
out-solformat      =llh        # (0:llh,1:xyz,2:enu,3:nmea)
out-outhead        =off        # (0:off,1:on)
out-outopt         =off        # (0:off,1:on)
out-timesys        =gpst       # (0:gpst,1:utc,2:jst)
out-timeform       =tow        # (0:tow,1:hms)
out-timendec       =3
out-degform        =deg        # (0:deg,1:dms)
out-fieldsep       =
out-height         =ellipsoidal # (0:ellipsoidal,1:geodetic)
out-geoid          =internal   # (0:internal,1:egm96,2:egm08_2.5,
3:egm08_1,4:gsi2000)
out-solstatic      =all        # (0:all,1:single)
out-nmeaintv1      =0          # (s)
out-nmeaintv2      =0          # (s)
out-outstat        =state        # (0:off,1:state,2:residual)
```

```
stats-eratio1      =100
stats-eratio2      =100
stats-errphase     =0.003      # (m)
stats-errphaseel   =0.003      # (m)
stats-errphasebl   =0          # (m/10km)
stats-errdoppler   =1          # (Hz)
stats-stdbias      =30         # (m)
stats-stdiono      =0.03       # (m)
stats-stdtrop      =0.3        # (m)
stats-prnaccelh    =10         # (m/s^2)
stats-prnaccelv    =10         # (m/s^2)
stats-prnbias      =0.0001     # (m)
stats-prniono      =0.001      # (m)
stats-prntrop      =0.0001     # (m)
stats-clkstab      =5e-12      # (s/s)
ant1-postype       =llh        # (0:llh,1:xyz,2:single,3:posfile,
4:rinexhead,5:rtcm)
ant1-pos1          =90         # (deg|m)
ant1-pos2          =0          # (deg|m)
ant1-pos3          =-6335367.6285 # (m|m)
ant1-anttype       =
ant1-antdele       =0          # (m)
ant1-antdeln       =0          # (m)
ant1-antdelu       =0          # (m)
ant2-postype       =llh        # (0:llh,1:xyz,2:single,3:posfile,
4:rinexhead,5:rtcm)
ant2-pos1          =90         # (deg|m)
ant2-pos2          =0          # (deg|m)
ant2-pos3          =-6335367.6285 # (m|m)
ant2-anttype       =
ant2-antdele       =0          # (m)
ant2-antdeln       =0          # (m)
ant2-antdelu       =0          # (m)
misc-timeinterp    =off        # (0:off,1:on)
misc-sbasatsel     =0          # (0:all)
misc-rnxopt1       =
misc-rnxopt2       =
file-satantfile    =
file-rcvantfile    =
file-staposfile    =
file-geoidfile     =
```

```
file-ionofile      =
file-dcbfile       =
file-eopfile       =
file-blqfile       =
file-tempdir       =/tmp/
file-geexefile     =
file-solstatfile   =
file-tracefile     =
#

inpstr1-type       =serial     # (0:off,1:serial,2:file,3:tcpsvr,
4:tcpcli,7:ntripcli,8:ftp,9:http)
inpstr2-type       =tcpcli     # (0:off,1:serial,2:file,3:tcpsvr,
4:tcpcli,7:ntripcli,8:ftp,9:http)
inpstr3-type       =off        # (0:off,1:serial,2:file,3:tcpsvr,
4:tcpcli,7:ntripcli,8:ftp,9:http)
inpstr1-path       =uart/2:115200:8:n:1:off
inpstr2-path       =:@10.0.60.51:50022/:
inpstr3-path       =
inpstr1-format     =ubx        # (0:rtcm2,1:rtcm3,2:oem4,3:oem3,
4:ubx,5:ss2,6:hemis,7:skytraq,
8:gw10,9:javad,10:nvs,11:binex,
12:rt17,15:sp3)
inpstr2-format     =ubx        # (0:rtcm2,1:rtcm3,2:oem4,3:oem3,
4:ubx,5:ss2,6:hemis,7:skytraq,
8:gw10,9:javad,10:nvs,11:binex,
12:rt17,15:sp3)
inpstr3-format     =rtcm2      # (0:rtcm2,1:rtcm3,2:oem4,3:oem3,
4:ubx,5:ss2,6:hemis,7:skytraq,
8:gw10,9:javad,10:nvs,11:binex,
12:rt17,15:sp3)
inpstr2-nmeareq    =off        # (0:off,1:latlon,2:single)
inpstr2-nmealat    =0          # (deg)
inpstr2-nmealon    =0          # (deg)
outstr1-type       =serial        # (0:off,1:serial,2:file,3:tcpsvr,
4:tcpcli,6:ntripsvr)
outstr2-type       =file        # (0:off,1:serial,2:file,3:tcpsvr,
4:tcpcli,6:ntripsvr)
outstr1-path       =../tmp/ttyV0:115200:8:n:1:off
outstr2-path       =/opt/lsts/rtklib/log/rtklib_output%Y%m%d%h%M.pos
outstr1-format     =enu        # (0:llh,1:xyz,2:enu,3:nmea)
```

```
outstr2-format     =enu        # (0:llh,1:xyz,2:enu,3:nmea)
logstr1-type       =file        # (0:off,1:serial,2:file,3:tcpsvr,
4:tcpcli,6:ntripsvr)
logstr2-type       =file        # (0:off,1:serial,2:file,3:tcpsvr,
4:tcpcli,6:ntripsvr)
logstr3-type       =off        # (0:off,1:serial,2:file,3:tcpsvr,
4:tcpcli,6:ntripsvr)
logstr1-path       =/opt/lsts/rtklib/log/
rtklib_ubxstream_x8_log%Y%m%d%h%M.ubx
logstr2-path       =/opt/lsts/rtklib/log/
rtklib_ubxstream_base_log%Y%m%d%h%M.ubx
logstr3-path       =
misc-svrcycle      =50         # (ms)
misc-timeout       =30000      # (ms)
misc-reconnect     =30000      # (ms)
misc-nmeacycle     =5000       # (ms)
misc-buffsize      =32768      # (bytes)
misc-navmsgsel     =all        # (0:all,1:rover,2:base,3:corr)
misc-proxyaddr     =
misc-fswapmargin   =30         # (s)
#misc-startcmd =./rtkstart.sh
#misc.startcmd =./rtkshut.sh
file-cmdfile1 =/etc/rtklib/data/ubx_raw_10hz.cmd
file-cmdfile2 =/etc/rtklib/data/ubx_raw_10hz.cmd
```